KU LEUVEN
FACULTY OF ECONOMICS AND BUSINESS

FACULTY OF ECONOMICS AND BUSINESS

A Practitioner's Guide to a Flood Risk Assessment

Building forward-looking flood maps for insurance applications

Yelle Hunninck

R0718216

Thesis submitted to obtain the degree of

MASTER OF ACTUARIAL AND FINANCIAL ENGINEERING

Promoter: Prof. Dr. Katrien Antonio
Work leader: Eva Verschueren

Academic year 2021-2022

KU LEUVEN
FACULTY OF ECONOMICS AND BUSINESS

FACULTY OF ECONOMICS AND BUSINESS

A Practitioner's Guide to a Flood Risk Assessment

Building forward-looking flood maps for insurance applications

Abstract

We develop a practical method to assess an insurer's proneness to flood risk, considering all the constraints a modern insurer faces, such as data scarcity, money, time and computational power.

In a first step, we modify current flood maps, providing a current view on flood risk, to provide a forward-looking view on future flood risk. Therefore, we develop an algorithm taking into account climate change data. Since there is a lot of uncertainty surrounding climate change evolution, scenario analysis is used as a flexible 'what if' framework to examine impacts based on different possible climate outcomes.

In a second step, we develop a white box method to assess proneness to floods using the developed flood maps. We compare this method to a black box method often used in practice.

In a final step, we argue how the developed flood maps can be integrated into an insurer's day-to-day processes, adding value to risk management, pricing and underwriting.

Yelle Hunninck
R0718216

Thesis submitted to obtain the degree of
MASTER OF ACTUARIAL AND FINANCIAL ENGINEERING

Promoter: Prof. Dr. Katrien Antonio
Work leader: Eva Verschueren

Academic year 2021-2022

Acknowledgements

This thesis would not have been possible without Saidja Vervaet and Lies Lierman. I am extremely grateful to them for providing me with the opportunity to experience how a modern insurer deals with flood risk. I would also like to express my thanks to Andrea Cascone, for guiding me through all technical aspects of developing, testing and applying flood models. Special thanks also go to Katrien Antonio, my promotor, and Eva Verschueren, my work leader, for providing feedback along the way. They contributed significantly to the quality of this paper. I would also like to thank my family and friends, who have helped proof-read and provide support throughout the year.

Table of Contents

General Introduction

Environmental, Social & Governance (ESG) risks are top of mind at the Belgian insurers. Especially climate risks, which can be cataloged under the environmental pillar of ESG, are prioritized. Climate risks are those risks arising from climate change. This can range from physical risks such as flooding or subsidence to transition risks which arise from disruptions and shifts associated with the transition to a low-carbon or environmentally sustainable economy. Increased carbon-related regulation is a prime example of this latter risk.

Climate risks may lead to significant increases in the claims received by insurers and can affect a variety of insurance policies. Since this can have far going implications on the underwriting profitability of insurers, the impact of climate change has been widely researched in actuarial literature. Climate change could, on the one hand, increase the occurrence of certain diseases like cancer, asthma or temperature-related conditions in the elderly population (International Actuarial Association, 2017). Also, climate-induced drought problems could affect production of food leading to famine. These effects would lead to mayor changes in mortality and would affect, for example, life insurances and pension products (Ford et al., 2019). On the other hand, property and causality actuaries could experience a real strain on their underwriting profitability if they are not able to adapt premia to reflect the increasing risk policyholders face or if reinsurance premia increase disproportionally (Tesselaar et al., 2020). Fire insurance, for example, which covers the material damages of, o.a., floods, wind storms and fires in Belgium, could be highly impacted, especially when considering the recent incidents in Western Europe like the exceptional rainfall resulting in disastrous floods during the summer of 2021 and the series of heatwaves in 2019. These events clearly illustrate that the frequency and severity of the events covered are already increasing.

This potential impact on the underwriting profitability and by extension the solvability of insurance companies has put climate risks high on the agenda of regulatory bodies like the National Bank of Belgium (NBB) and the European Insurance and Occupational Pensions Authority (EIOPA). EOIPA recently issued several papers on the possible inclusion of climate risk in Solvency 2 and the Own Risk and Solvency Assessment (ORSA) (Delcea, 2020; Delcea, 2021). Also, the Institute and Faculty of Actuaries (IFoA) stresses the importance of climate risk informed decision making. In a risk alert, a tool used to highlight important topics to its members, they emphasized that actuaries must always consider how climate-related risks could affect their business (IFoA, 2017). Moreover, they voiced that actuaries should assess the impact to the best of their abilities while remaining transparent on which parts of their analyses already incorporate climate risks and which parts lack integration.

Scenario analysis is a tool often used by actuaries to transparently assess impacts in climate related analyses. The main reason of this use is that climate change is surrounded by a lot of uncertainty. Many scenarios are still possible, depending on the actions we take now and in the future. Hence, scenario analysis allows to examine impacts based on different possible climate outcomes. These different outcomes are often called climate pathways. Many frameworks have been developed describing different pathways. The Network for Greening the Financial System (NGFS) is a well-known framework that is often used by practitioners and is endorsed by regulators.[1] EIOPA is an important member of the initiative and suggests the use of the framework in, a.o., the own risk and solvency assessment (ORSA) and stress testing (Delcea, 2020; Delcea, 2021). Also in literature, the NGFS framework is often used. Bongiorno et al. (2022) published a paper on how pension actuaries can use climate scenario analysis to assess future risks and opportunities in defined benefit schemes. They relied on the Climate Maps Pathways, which are mainly based on the NGFS framework. Another, often used framework is the Representative Concentration Pathways (RCP). The RCP are used by the United Nations Intergovernmental Panel on Climate Change (IPCC) in its climate change reports (IPCC, 2021). Those reports are generally considered by practitioners and scientists as one of the most complete descriptions of climate change impacts and outcomes.

An impact assessment under different scenarios is no straightforward exercise since current frameworks and processes often lack climate integration. (Re)Insurers will have to revise, a.o., their underwriting, pricing, risk management and reserving processes, to fully incorporate climate risks. Next to these, reinsurance processes as well could benefit from climate risk adaption. Rothwell et al. (2020) explain that due to an increased uncertainty in claims expenditures, reinsurance requirements may change. An insurer which has already incorporated climate related risks in their risk assessment may be better placed to manage those changed requirements and monitor and renegotiate reinsurance contracts.

The integration of climate risk is a very time consuming and gradual process. Hence, prioritizing the most significant risks at the start is key. Flood risk is one of the physical climate risks Belgian insurers expect to be especially prone to. This has several reasons. Firstly, the Joint Research Center (JRC), a science and knowledge task force of the European Commission, has indicated that river flooding is the costliest natural catastrophe event in Europe (Dottori et al., 2020). Also, the JRC expects floods to be responsible for the highest economic cost due to climate change. If climate change is not appropriately managed by taking suitable measures, direct damages could increase up to six times their current level in Europe, by 2100 (Dottori et al., 2020). Secondly, brokers, providing natural catastrophe model solutions, have also indicated that they perceive inland river floods as the most important climate risk (personal communication, 17 February

[1] For more information on the NGFS pathways visit https://www.ngfs.net/en

2022). They base their claim on the Clausius-Clapeyron relation, which models the atmospheres capacity of holding water at certain surface temperatures (Brown,1951). This capacity increases non-linearly with global warming. A one degree increase in surface water could constitute six to seven percent more water vapor (see e.g. Risser & Wehner, 2017). This could have a substantial impact on the amount of rainfall.[2] Hence, brokers predict a significant increase of gross losses, i.e. losses taking into account all policy stipulations but no reinsurance, of more than 40% by 2086. Finally, most Belgian people, whose properties are covered for flood damages under a fire insurance policy, live in Flanders. Due to its flat geography, land use, and dense population, insurers expects Flanders to be particularly susceptible to this peril. Recent research by the Vlaamse Maatschappij voor Milieu (VMM), the Flemish governmental organization responsible for all aspects of climate and environment, supports this concern by indicating that the number of buildings affected by floods could double by 2050.[3] For these three reasons, insurers have prioritized the impact analysis of current and expected future floods on their flood covering fire insurance portfolios, over other natural catastrophe events.

Flood risk can be assessed during a flood risk analysis. Such a study requires specialized data from a multitude of public, private and company sources. However, this data often lacks the necessary granularity to assess risks accurately. Moreover, it is often not yet present. This can be attributed to the fact that, in the past, practitioners had no reason to systematically gather, process and analyze flood relevant data for insurance. A prime example of essential data which is often missing are flood maps. All these impact assessments rely significantly on them since they give insight into the extent, severity and probability of a particular theoretical flood. They serve as the basis for the calculation of flood losses. Current flood maps are constructed based solely on known and certain climatological information, while future flood maps take climatological projections into account. Hence, they provide a forward looking view on flood risk. The method of constructing these maps is very dependent on the landscape under investigation. Therefore, many different models exist and insurers often have to rely on local governments to provide the maps. However, many governments do not want or are unable to share their flood maps, making it very difficult for insurers to perform their own flood analysis. Especially forward looking maps are scarce. In Belgium, only the Flemish government supplies these kind of maps. Countries like Bulgaria, Poland, Czechia and Hungary, do not report any maps. Consequently, future flood maps regularly constrain the success of impact assessments.

---

[2] For more information on Clausius-Clapeyron and climate risk see e.g. https://www.jbarisk.com/news-blogs/the-physics-of-precipitation-in-a-warming-climate/

[3] For more information: https://klimaat.vmm.be/themas/overstromingen

Many brokers and reinsurers have tried to offer a solution to this problem by developing their own flood maps and incorporating them in flood risk assessment tools (e.g. Q-FLAT from Aon; G-CAT from Guy Carpenter). These tools are often used by insurers to estimate their proneness to floods. Figure 1 shows the normal course of such a process. The insurer first gathers data on all policyholders insured for flood. This data ranges from addresses to specific policy information like retention limits. The insurer then sends this data to the broker. The broker uses this as input in its model and sends back information on the insurer's total flood risk. This is often referred to as an expected flood claim or damage factor. This output can then be used in several processes like pricing, underwriting and reserving. A major disadvantage of broker tools is that the results are very black box since brokers often only report on end results and do not go into the details of the methodology. This can lead to significant interpretability issues when incorporating the insights in an insurer's day-to-day business. Insurers that require more insight in their flood risk have to develop their own models. However, literature does not offer much guidance on how such a model could be build using the constraints of time, data, computational power and money a typical insurer faces.

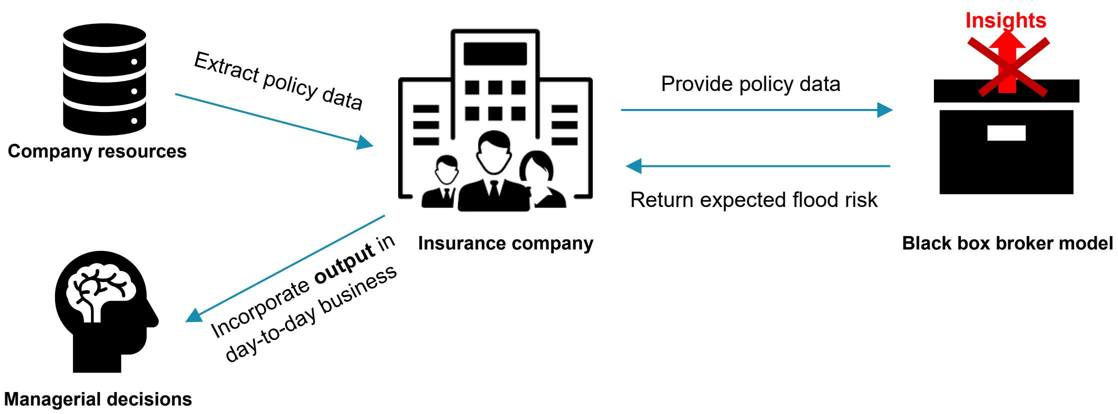

Figure 1: The flood risk analysis process when performed using a proprietary black box model from a broker or reinsurer.

This paper fills this important gap in literature. It not only provides a practitioners guide to a feasible flood risk assessment, taking into account the needs of modern insurers, it also develops a brand-new algorithm to construct future flood maps. This algorithm is developed such that it can be easily implemented and integrated into the day-to-day business of practitioners. Moreover, since the algorithm only relies on publicly available resources, the success of the flood risk assessment is not contingent anymore on local governments, brokers and reinsurers providing data or models.

Figure 2 visualizes the setup of the flood risk assessment methodology and shows which chapters of this paper will detail which parts.

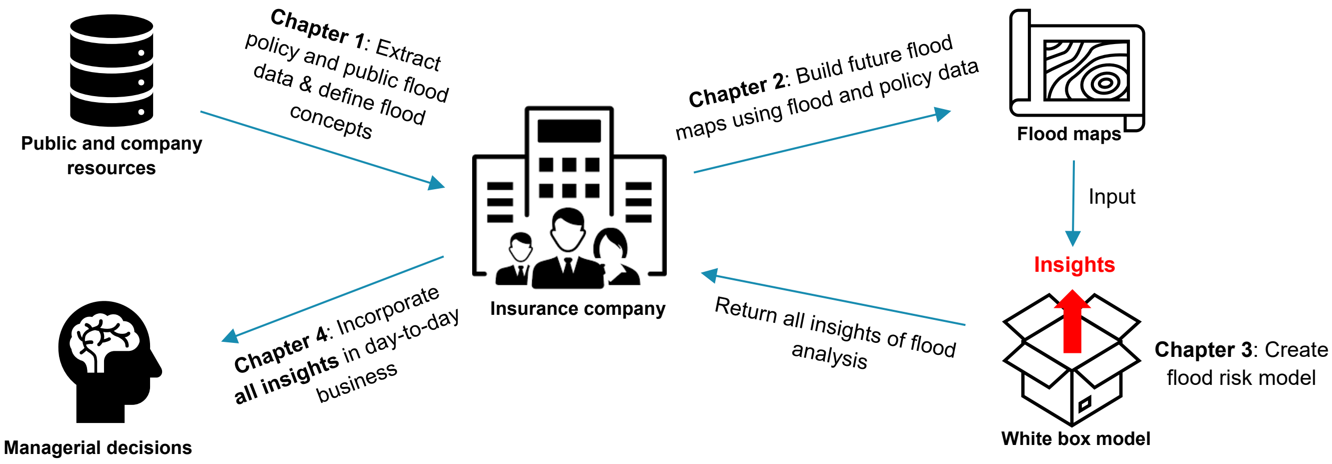

Figure 2: Flood risk analysis process as developed in this paper making use of only publicly available data.

Chapter 1 of this paper will define the most important flood risk concepts. An unambiguous view of the concepts is essential when interpreting final results.

Chapter 2 develops a novel algorithm to construct own future flood maps since these are often not publicly accessible. The different subsections detail all necessary steps of the algorithm, exposing potential shortcoming and strengths. Our aim is twofold. Firstly, we strive for these maps to have sufficient accuracy such that the resulting estimate of proneness to flood risk can be used in, for example, the ORSA or as a tool for the underwriting of contracts, the pricing of products, the setting of retention limits for reinsurance contracts or comparison with broker models. Secondly, the method should allow building these maps, spanning large areas, often whole countries, with limited resources. Especially computational power and time are two important aspects in this respect.

Chapter 3 develops a white box flood risk assessment model using the built flood maps. This model is compared to the black box broker model often used by insurers in practice. Special attention will go to pointing out not only the elements our model improves on but also the weaknesses and parts that need further research.

Finally, chapter 4 concludes by proposing several applications of the flood maps and flood model in an insurers day-to-day business. We indicate how they can be incorporated in, for example, the risk management, pricing and underwriting frameworks.

1 Flood risk analysis concepts

This chapter defines the most important concepts specific to a flood risk assessment. We start by looking at the Digital Elevation Model (DEM) in section 1.1. This model is the basis of any flood risk analysis. Since climate change is surrounded by a lot of uncertainty, it is essential to report on the climate change assumptions leading to the results. Hence, section 1.2 introduces the framework of the Network for Greening the Financial System (NGFS). This framework describes different possible future climate states and is used to disclose climate assumptions. Section 1.3 analyzes the structural components of flood risk. A particular focus is put on unambiguously defining the meaning of these components as they are often interpreted differently in literature. We follow similar definitions as the ones introduced by Kron (2005). The different subsections further elaborate on the details of these components.

1.1 Digital Elevation Model

A Digital Elevation Model (DEM) topographically describes a 3D view of the terrain. Hence, it can be used to represent a landscape. Figure 3 gives a visual representation of such a DEM on a small scale. The map is comprised of many individual points, each representing a location in the landscape. The x and y coordinates of the points define the longitude and latitude. The z coordinate provides information on the elevation of the point with respect to sea level. In Figure 3, this is visualized using a color scheme, where lighter colors indicate higher grounds. The density of the points per area is called the granularity ("horizontal resolution"). Typical DEMs, used by practitioners, consist of points spaced 25 – 30 meters apart. The DEM in Figure 3 has such a granularity.

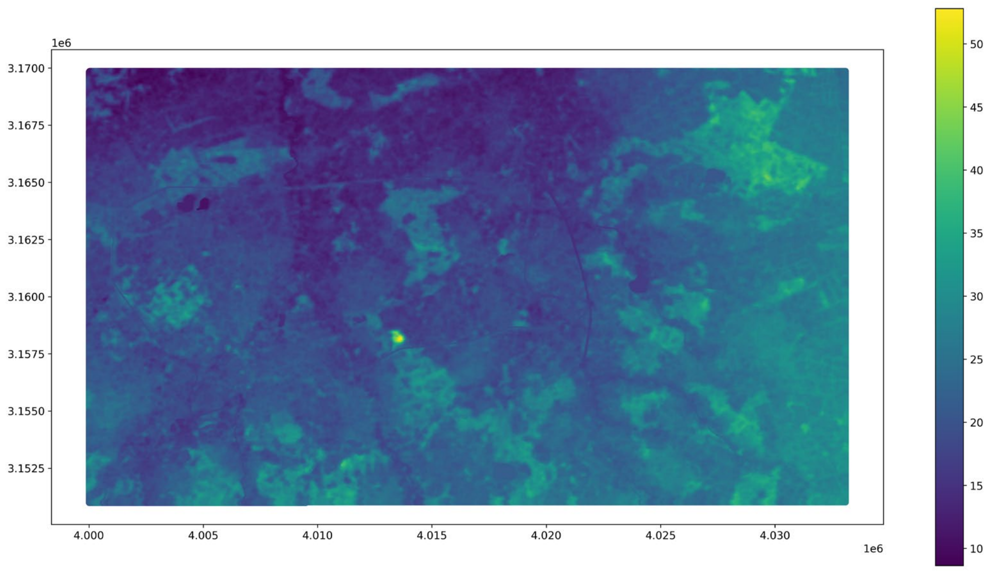

Figure 3: Snapshot of the EU Digital Elevation Model.

A DEM differs from a Digital Surface Model since it makes abstraction of any objects like buildings, bridges, forests or water bodies.[4] It is a critical component of many geographical studies, such as a flood risk study, because its accuracy of representing the landscape is a significant determinant of the trustworthiness of the results (Sampson et al., 2016). The accuracy of a DEM is often measured as the Root Mean Squared Error (RMSE) of the vertical accuracy and can be defined by:

$$RMSE = \sqrt{\frac{1}{n}\sum_{i=0}^{n}(Observed_i - DEM_i)^2}.$$

In this formula the index i runs over the n 3D points used to represent the landscape in the DEM. Consequently, a more granular DEM will have a higher n, since it has a higher point density. The RMSE will compare for all points the theoretical elevation of the DEM, DEM_i, and the actual elevation measured on site, $Observed_i$, by computing the average squared differences. Hence, the RMSE provides intuition into how accurate the DEM model can represent the landscape. If large discrepancies exist between the theoretical and actual elevations, the RMSE will be high. If the DEM is a perfect representation, the RMSE will be zero. Consequently, DEMS with low RMSEs are preferred.

The European Commission has set out to develop a European DEM with an RMSE below 7 meters (Dufourmont et al., 2014). Such initiatives to develop accurate DEMS are essential since inaccuracy in the terrain measurement can lead to undesirable variability in elements derived from the DEM, like inundation depth or flood extent.

Consequently, increasing demand by practitioners and regulators resulted in more accurate DEMs. Scientists have devised new technologies to comply with this request (Yamazaki et al., 2017). A favored new DEM uses radar interferometry and goes by the name of the Shuttle Radar Topography Mission (SRTM) DEM (Rabus et al., 2003). Another broadly used technology is based on stereo viewing of optical satellite images. A DEM developed in this respect is the Advanced Spaceborne Thermal Emission and Reflection Radiometer-Global DEM (ASTER GDEM) (Abrams, 2000). Many other promising technologies exist and are being developed (see, e.g., Mason et al., 2015).

Some projects combine multiple DEMS to further decrease the vertical RMSE. The Digital Elevation Model over Europe (EU-DEM) is an example (Dufourmont et al., 2014). The Copernicus program has developed this DEM by combining SRTM DEM and ASTER GDEM datasets. The EU-DEM is Europe's answer to the increasing need for a pan-European high-quality DEM. Validation of the model has

[4] https://ec.europa.eu/eurostat/web/gisco/geodata/reference-data/elevation

shown that it can achieve an overall vertical RMSE of 2.7 m at a 90% confidence level. This is well below the 7 meters set out by the European commission in 2009. Hence, the model is quite accurate. As the name suggests, this particular DEM spans the whole of Europe. Moreover it is free to download, making it a perfect candidate to use in the construction of future flood maps, discussed in chapter 2. Figure 3, displayed at the beginning of this section is a snapshot of the EU-DEM at a location close to Eindhoven in the Netherlands.

1.2 Network for Greening the Financial System: Climate pathways

Substantial uncertainty surrounds the evolution of climate change. Many scenarios are still possible, depending on the actions we take now and in the future. Hence, when an insurer must report on future climate risks, the results can be very diverse or even contradictory depending on the assumptions made. To avoid ambiguity, it is essential to clearly state the climate change assumptions or climate framework used when reporting on future risks to a stakeholder like EIOPA.

The framework of the Network of Central Banks and Supervisors for Greening the Financial System (NGFS) is broadly adopted by practitioners to report on climate related insurance topics, since the European regulator for insurers, EIOPA, is itself a member of the initiative (see recommendations to use the framework in, e.g., Delcea, 2020 and Delcea, 2021).[5] It is therefore a good choice for reporting purposes. The framework consists of six scenarios grouped in three dimensions: orderly, disorderly, and hot house world (Figure 4). The orderly scenarios start from the idea that early on decisive climate actions are taken on a global scale. These actions gradually become more stringent over time. This gradual approach will minimize both physical and transition risks. Contrary to this dimension, no global approach is found in the hot house world scenarios. Climate actions are therefore insufficient and lead to a surge in natural catastrophes. Physical risks are the highest in this scenario. The disorderly scenarios can be placed on the other end of the spectrum, where actions are taken, albeit delayed. This leads to a sudden increase in policy measures after some time. These actions are sufficient to avoid the physical risk experienced in the hot house world scenarios. However, new risks arise in the form of transition risks.

Chapter 3 will make extensive use of this framework to link the performed flood risk analysis to one of the three dimensions. This way, it is transparent for the

[5] For more information on the climate pathways visit https://www.ngfs.net/en

regulators which climate change assumptions have been made to come to the results.

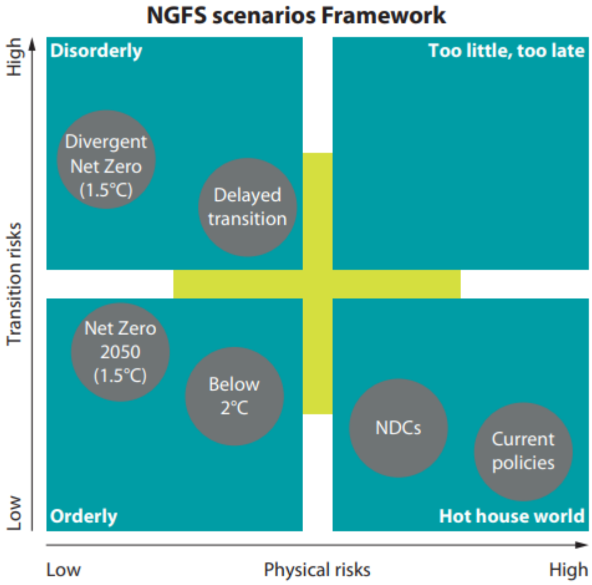

Figure 4: NGFS framework taken from NGFS.net.

1.3 Flood risk analysis

Flood risk is one of the most prioritized climate risks. Therefore, it is essential to have a thorough understanding of what a flood risk analysis entails. It generally consists of 3 components (Kron, 2005): hazard, exposure, and vulnerability.

1.3.1 Hazard

When analyzing the hazard, we want to understand floods as natural catastrophes. Questions we want to solve in a hazard analysis can be: with what frequency do floods occur? What is the expected flood extent? How does the inundation depth differ per area? What is the probability of observing this flood? The hazard thus provides information on the severity of a flood and associates it with a certain probability. The severity is often measured by a combination of the flood extent and the inundation depth. However, also other parameters like the velocity of water or speed at which the water rises can be used in this respect (de Moel et al., 2009). The probability describes the odds of the flood occurring in a year. Hence, it is a proxy for the frequency, since more probable flood will happen more frequently. This probability is often formulated as a yearly probability of observing a similar or worse flood. Hence, it is also called an exceedance probability (Humphreys, 2020). This information on probability of occurring and severity can be summarized in flood hazard maps.

Figure 5a and 5b illustrate the concept of flood hazard maps. Figure 5b provides information on the severity of the flood using the inundation depth. Here, darker colors indicate more inundated areas. The flood extent is also clearly delineated. The map has an associated exceedance probability of 1%. Figure 5a displays the effect of exceedance probability on the flood extent. We clearly see that lower probabilities, indicated by the lighter colors, lead to more extreme floods which will occur less often.

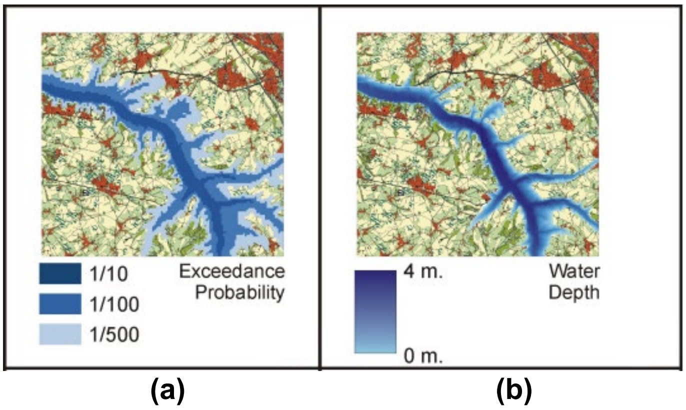

Figure 5: An example of a flood hazard map. (a) A visualization of the difference in flood extent for different exceedance probabilities. (b) An illustration of the difference in depth across a flood with a specific return period. This picture is taken from the paper of de Moel et al. (2009).

Flood hazard maps can display a current or a future view. Current maps take into account all available current climatological knowledge. They thus provide information about the flood hazard experienced at the present moment. On the other hand, future maps extend the current maps by making assumptions about the future climatological situation. Depending on these assumptions, future maps can differ widely. Comparing the current and future maps can give some insight into how climate change will affect flood hazard.

Many different approaches exist to construct flood hazard maps. However, as de Moel et al. (2009) described, most follow the three steps described in the following paragraphs. These paragraphs are not exhaustive in their explanation, yet try to give intuition such that the algorithm in chapter 2, where we construct future flood maps, can be better interpreted.

Step 1: Estimate river discharges

First, the modeler wants to get insight into river discharges for different return periods. The discharge of a river describes how much water flows through a river at a specific place. It is measured in m^3/s. The return period is a probability concept. It can be directly linked to the exceedance probability, described in the first paragraph, by the following relation: $Return\ Period = \frac{1}{Exceedance\ Probability}$ (Homer et al., 2017). Hence, the return period also describes the likelihood of occurrence. For example, a discharge of 30 m^3/s associated with a return period of 10 years means that every year there is a $1/10$ or 10% probability of observing a similar or worse discharge while a return period of 100 years means that the probability of exceedance is only 1% per year. Consequently, a higher return period is associated with more extreme discharge values. Note that, despite what the name suggests, a 10 year return period discharge cannot be interpreted as a discharge that is observed once every 10 years (Humphreys, 2020). It only refers to the annual exceedance probability, as explained above. If we want to know, for example, the probability that a 10 year discharge occurs at least once in 10 years, we have to rely on the Binomial distribution. The probability density function is given by:

$$P(k,n,p) = \binom{n}{k} * p^k * (1-p)^{n-k}.$$

In this situation it models the probability of observing the discharge (or worse) exactly k times over n years, where p is the yearly exceedance probability. Using this building block we can easily derive the probability of observing the discharge at least once by taking the complement of the probability that the discharge is never observed:

$$P(k \geq 1, n = 10, p = 0.1) = 1 - P(k = 0, n = 10, p = 0.1).$$

This is for a 10 year discharge equal to 65%.

A multitude of methods exist to estimate those discharges. One could, for example, use a hydrological model. This is often called a rainfall-runoff model (see, e.g., de Moel et al., 2009; Wright, 2015). We will only give some intuition into how such a model works, based on Figure 6.

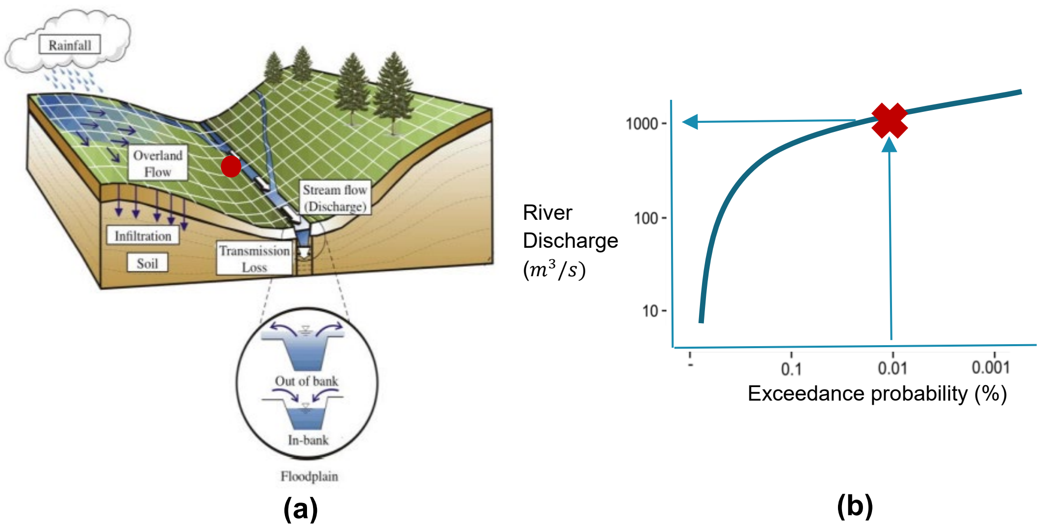

Figure 6: (a) Diagram of a rainfall-runoff model. This model can be used to estimate river discharges. (b) The output of the model. Figure a is taken from the paper of Wright et al. (2015) while Figure b is based on another figure of the same paper.

A rainfall-runoff model tries to model the hydrological features of water bodies like rivers or groundwater based on how rainfall and water run through the landscape. Hence, important elements in such a model are, for example, the infiltration capacity of the soil, visualized with the arrows pointing down from the surface, the geography of the landscape, displayed as a grid and estimates of rainfall. The grid is often represented by a DEM in practice. The rainfall estimates can be based on historical observations.

The rainfall-runoff model then calculates discharges associated to different exceedance probabilities as can be seen in Figure 6b. It does this by simulating discharges for different rain intensities, that are linked to particular probabilities of occurring. In Figure 6a, this is intuitively displayed as the runoff of rainfall across the hill to the stream. Hence, the name rainfall-runoff model. Figure 6b shows the output of the rainfall-runoff model calibrated at one particular point in the landscape. This point is indicated with a red dot in Figure 6a. The red cross for example tells us that at the red dot we have a 1% probability each year to observe a discharge of 1000 m^3/s or more.

Step 2: Convert river discharges into water levels

The first step in building a flood hazard map, the basis of all flood risk analyses, is now complete. We can now continue by converting the resulting discharge rates into river water levels, also called flood stages. This step is important because the depth of the water is used as an important determinant of the severity of a flood. In section 1.3.3, the depth will prove to be crucial in determining a final flood loss. Moreover, the depth is often used to determine the final extent of the flood. Intuitively, we expect that more significant flood stages will be associated with more extreme river discharges and wider flood extents, since a discharge represents the amount of water that flows through a river. Figure 7 visualizes how static stage-discharge functions can be used to convert discharges into river depths. The function on the left is such a stage-discharge function. It relates the discharge observed in a part of the river (y-axis) to the water stage at that location (x-axis). It is often calibrated on historical observations. In this example, a discharge of around 1000 m^3/s, leads to a depth of just below 6 meters, as is indicated by the arrows.

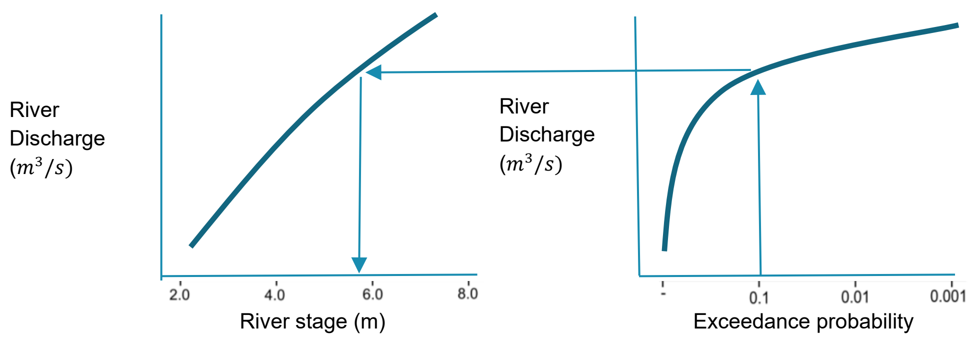

Figure 7: A graphical representation of how a static stage-discharge function (left) can be used to transform river discharges (right), simulated by the rainfall-runoff model, into river stages. This method and illustration is based on the paper of Wright et al. (2015).

Instead of static functions, one could also opt for more dynamic hydrodynamic models, considering other factors like flow velocity, soil composition, or flood duration (see, e.g., de Moel et al., 2009; Wright, 2015).

Step 3: Determine flood extent based on calculated depths

After step 2, we know the depth of the water at different places in the landscape. However, we do not yet know how far this water would flow and where the flooding would stop. Hence, a final step in building the flood map uses these depths to calculate the flood extent. The most straightforward method is based on an interpolation/intersection technique (see, e.g., Apel et al., 2009; Wright, 2015). The method is visually displayed in Figure 8. We start by projecting the derived water levels on the landscape, illustrated as floating red points in Figure 8a. These red points are then transformed into a sloping flood plain by connecting them in Figure 8b. Finally, this flood plain is intersected with the landscape. This locks the extent of the flood and is illustrated in blue Figure 8c. This paper will base the building of forward looking flood maps on this approach in chapter 3. More advanced methods, using hydrodynamic models, can automatically output the extent and depth on a map since the DEM is used as an input of the model.

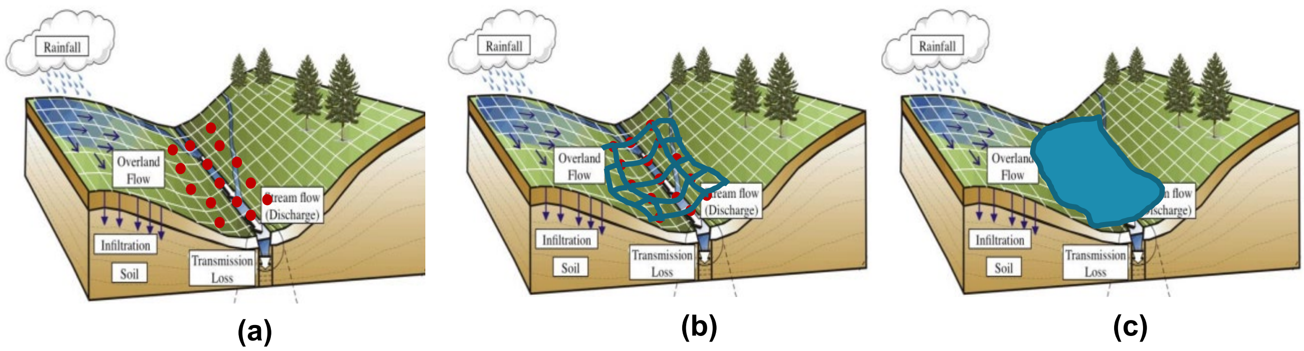

Figure 8: Illustration of the intersection/interpolation technique. The illustrations are based on Wright et al. (2015).

The interpolation technique is considered to be a simple approach. Added complexity will, in most cases, lead to more accurate results. Apel et al. (2009) illustrate this clearly in their paper, comparing three hydrological models of varying complexity. They found that the more complex models outperformed the more straightforward approaches when comparing the flood extent and inundation depth to some benchmark. Nevertheless, the interpolation technique also provided a reasonable estimate of the flood extent and inundation depth at a much lower overhead. Only at smaller inundation depths did it tend to overestimate results. Even though this technique performed well in the examined area, the author cautions that this strategy is not recommended for use in mountainous or flat lowland regions since hydrological concepts will become very important to accurately capture the flood characteristics in these terrains. This will be an essential finding to keep in mind when analyzing the flood risk of an insurer having considerate property exposure to flat lowland regions, like Flanders or the Netherlands, in their fire insurance portfolio.

The paper by Apel et al. (2009) also found that the quality of the results is reasonably susceptible to the accuracy of the hazard model. However, when combining the hazard model with some vulnerability model, used to estimate the total flood loss, they found that the accuracy of the hazard model was less important than the method of calculating the loss. They thus concluded that the hazard modeling accuracy has a minor impact compared to the accuracy of the flood loss model. These models will be the topic of section 1.3.3, describing the vulnerability component.

1.3.2 Exposure

The exposure of a flood event relates to the buildings, objects, or persons who possibly suffer damages due to a flood event (Kron, 2005). However, the exposure is highly dependent on the specific situation. Private persons' exposure can be limited to their house, belongings, and family present in the building during the flood, while the exposure of an insurer depends heavily on the specific extent of the coverages he offers as well as on the composition of his portfolio. Some insurers may have significant exposure to floods, i.e., they have many fire insurance policies in their portfolio, limited reinsurance, or a higher concentration of buildings in flood-prone areas, while others can have no exposure. For example, absence of flood exposure can occur when an insurer focuses only on a specific type of cover, e.g., pet insurance.

Flood hazard maps can be used to assess current and evaluate future exposure. An insurer can evaluate his exposure by mapping his flood covering portfolio onto current and future flood maps. Analyzing the current number of properties at risk and the possible increase due to climate change can give a clear risk signal to management. However, the exposure is only one piece of information. Even more important is knowing how the damages associated with this exposure could evolve. The vulnerability captures this element.

1.3.3 Vulnerability

The vulnerability captures how vulnerable the assets at risk are when they are flooded (Kron, 2005). It thus models the damage of a flood, often expressed as a monetary value. The extent of the damage can depend on a variety of things. Firstly, preventive flood protection measures can significantly mitigate the total loss. Possible measures are sandbags or drainage systems. Secondly, also the use of buildings can have a considerable impact. When hit by a comparable flood, residential buildings are expected to have a lower loss than an industrial, agricultural or commercial site. This is on the one hand due to the expensive and complex to replace equipment present at such sites. This machinery is often present on the ground floor, which adds to the loss. On the other hand, the business continuity of a company is compromised when the equipment is unavailable. This can also be a significant contributing factor to the total loss, albeit an indirect source of damage.

Many models and techniques exist to capture the relationship between the flood's severity and the asset's loss (Molinari et al., 2020). Each model is tailored to a specific use. Some models, for example, try to be as commonly applicable as possible. Hence, they are primarily useful when evaluating the loss of buildings spread over a larger geographical area, such as large countries. In chapter 3, we will make extensive use of a model having this characteristic since we want to evaluate flood risk on a country level.

Vulnerability models also differ widely in complexity (Molinari et al., 2020). The simplest models only take one variable into account and are fitted to empirical loss data of past floods. Inundation depth is a variable used extensively in this respect. After calibration, the model could then predict the loss associated to a certain flood stage in function of the sum insured (SI) as:

$$Expected\ flood\ loss = \begin{cases} x\,\% * SI & if\ \ flood\ depth < a \\ y\,\% * SI & if\ \ a\ \leq flood\ depth < a+1 \\ z\,\% * SI & if\ \ flood\ depth \geq a+1 \end{cases},$$

$$with\ 0 \leq x, y, z \leq 100\ \ and\ \ a \geq 0.$$

(Equation 1)

In this fictitious example, a flood depth of $a + 0.5$ meters would lead to an expected claim size of y % of the property’s sum insured. Even these low-variable models can become very complex when replacing the empirical damage function with a parametric model. The Weibull and beta distributions are often choices made by modelers in this case (Balica et al., 2013).

The various flood vulnerability models can be generally split into three categories: vulnerability matrices, vulnerability indicators, and vulnerability curves (Papathoma-Köhle et al., 2015). We will only focus on the vulnerability curves since these are the most often used when evaluating the vulnerability at a large scale, which we will do in this paper.

Depth-Damage curves are univariable loss models that practitioners widely embrace for their simplicity (see, e.g., Huizinga et al., 2017; Gerl et al., 2016 or Molinari et al., 2020). These functions relate the damage of a building and its household to the severity of the flood expressed in inundation depth. They express this relation as a percentage of the total sum insured. Hence, Equation 1 was a very simple example of such a depth-damage curve. Insurance companies can fit these curves to historical loss datasets. However, in many cases an inadequate amount of data points are present to properly calibrate the model. Therefore, market data gathered by reinsurers or governments is often used. Figure 9 shows a selection of calibrated curves on market data for a variety of European countries. The depth of the flood at a specific residential property is indicated on the x-axis, while the damage factor, i.e. the percentage of the sum insured at risk, is displayed on the y-axis. Selecting the blue dotted Belgian curve, an insurer expects on average a claim size of 20% of the sum insured of a Belgian residential property, when it is flooded by a depth of 1 meter.

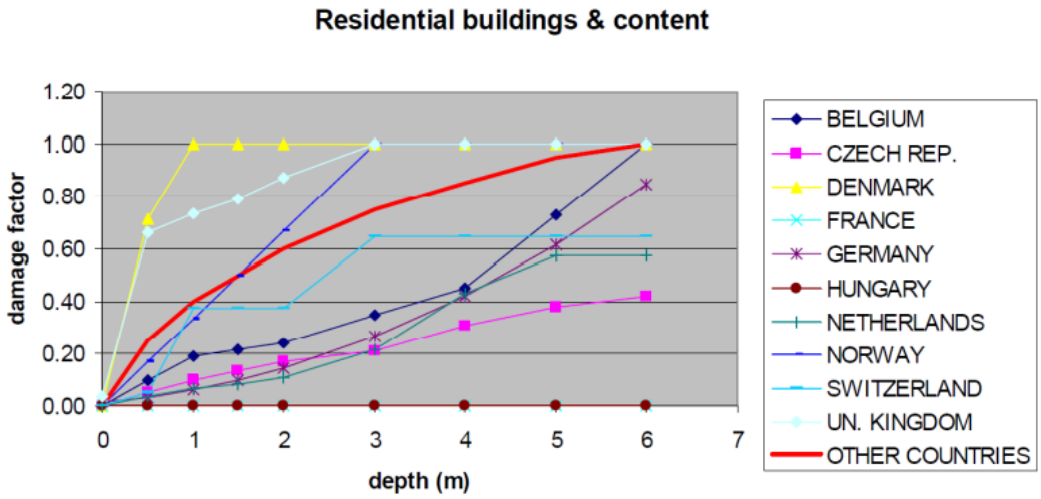

Figure 9: A selection of calibrated depth-damage curves, taken from the paper of Huizinga et al. (2017).

A drawback of these curves is that they tend to underestimate losses when used in seclusion, since they cannot accurately assess damages related to the structure of the building (Mediero et al., 2021). To achieve this, other factors like flood velocity and duration have to be taken into account. Nonetheless, they are very popular among practitioners because of their simplicity and general applicability.

Important to note is that at the moment of writing, only few vulnerability models take flood velocity and duration into account in practice (personal communication with Guy Carpenter, February 2022). Consequently, when modeling the severe flood losses in Wallonia in 2021, the damages were on average considerably underestimated. This was caused because during that specific flood, the velocity of the water rushing from the rocks and hills was a significant contributor to the total flood loss. Hence, velocity was an important predictive variable that was not taken into account.

2 Building forward looking flood maps

Often, data scarcity limits the success of a flood risk assessment. An important element which is frequently missing are future flood maps. These maps represent the severity and frequency of future floods based on some estimate of the future climatological situation. Since these maps are most of the time not available, this paper proposes a novel method to construct them from publicly available data. This way, insurers are not dependent anymore on local governments to supply the maps.

In this chapter we will provide a detailed overview of how the forward-looking flood maps are constructed. The technique used is based on the general idea of interpolation as described in section 1.3.1. First, section 2.1 will introduce and describe the two publicly available datasets used as input data by the algorithm. We will zoom in on their structure and main assumptions. This information is essential to understand the modeling decisions described in section 2.2. We will provide insight in the preliminary results of the algorithm on a small subsample of the data, presented in section 2.3. We will also provide a critical view, exposing the potential flaws and areas where the proposed technique could be improved. The last section will go deeper into some of the assumptions we made to build the maps.

2.1 Data analysis and processing

2.1.1 Digital elevation model

The first dataset used by the algorithm is the digital elevation model developed under the Copernicus program and provided by Eurostat, i.e. the EU-DEM. As previously explained in section 1.1, it is composed of many 3D points that have a longitude, latitude and elevation. Together, they give a 3D view of the landscape across Europe (See Figure 3). The EU-DEM is quite accurate having an overall RMSE of 2.9 meters across all European countries and an RMSE of 1.58 meters in Belgium. Hence, both are well below the seven meters set out by the European Commission in 2009 (Dufourmont et al., 2014).

Table 1 provides some insight in the dataset. It describes the 3D points based on 2 attributes: the geometry, which represents specific locations in the landscape using longitude and latitude values, and the elevation, which shows the elevation at those coordinates. We have tabled 5 of the more than 50 million points that make up Flanders in Table 1.

Index	Geometry (Longitude Latitude)	Elevation (m)
1	POINT (4000062.5 3169862.5)	10.44
2	POINT (4000087.5 3169862.5)	10.88
3	POINT (4000112.5 3169862.5)	11.81
4	POINT (4000137.5 3169862.5)	12.84
5	POINT (4000162.5 3169862.5)	13.83

Table 1: Example of the EU-DEM Dataset (Copernicus program, 2016).

2.1.2 Joint Research Center flood maps

The second dataset describes flood hazard in Europe. It is developed by the Joint Research Committee. Throughout this paper, we will refer to these flood hazard maps as the JRC maps.

Table 2 provides some insight in the dataset. We have 2 columns containing severity data, namely geometry and depth. The first column describes the shape of the flood extent. This extent is comprised of many polygons representing floodplains in the landscape of an equal flooding depth. This depth is derived from river discharges as was described in section 1.3.1. Figure 10 gives an illustration of how this would look like around a small part of the Flemish river the Schelde. We see that the blue floodplains range from squares and rectangles to more elaborate shapes. Together, they denote the full flood extent. Important to note is that the smallest floodplain in the dataset is a square with sides of 100 meter. All others are constructed by a multiple of these squares. For example, the rectangle P1, in Figure 10, is comprised of 2 squares. Hence it has a width of 200 and a length of 100 meters. We can also observe that none of the polygons overlap. The second attribute in the dataset specifies the inundation depth in each floodplain.

Index	Geometry (Coordinates)	Depth (m)
1	POLYGON ((141112.3647195539 224891.6856643194, 141212.1252370884 224899.3931359621, 141227.4950498162 224700.0680699199, 141127.7345775824 224692.3606546409, 141112.3647195539 224891.6856643194))	0.25
2	POLYGON ((141311.8857341288 224907.1005774215, 141511.4066667509 224922.5153697804, 141526.7763435464 224723.1901347274, 141626.5367338192 224730.8974293116, 141634.2214343041 224631.2348063299, 141334.9402699262 224608.1129165189, 141311.8857341288 224907.1005774215))	0.07

Table 2: Extract of the JRC 10 year return period dataset (Dottori et al., 2021).

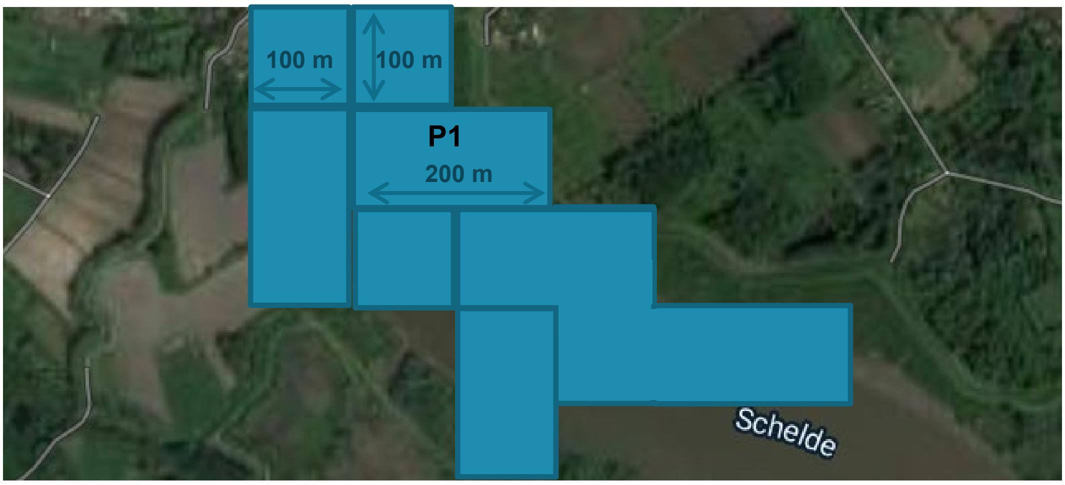

Figure 10: A visual representation of how polygons in the JRC maps could denote the extent of a specific flood of the Flemish river the Schelde.

The JRC maps also report on the associated probability, since the maps are available in different return periods of 10, 100 and 500 years. The more probable situation the flood map depicts, the lower the return period will be. A flood map which is more probable often has a smaller flood extent and inundation depth. Figure 11 shows the difference in extent between the Flanders' ten and hundred return period maps.

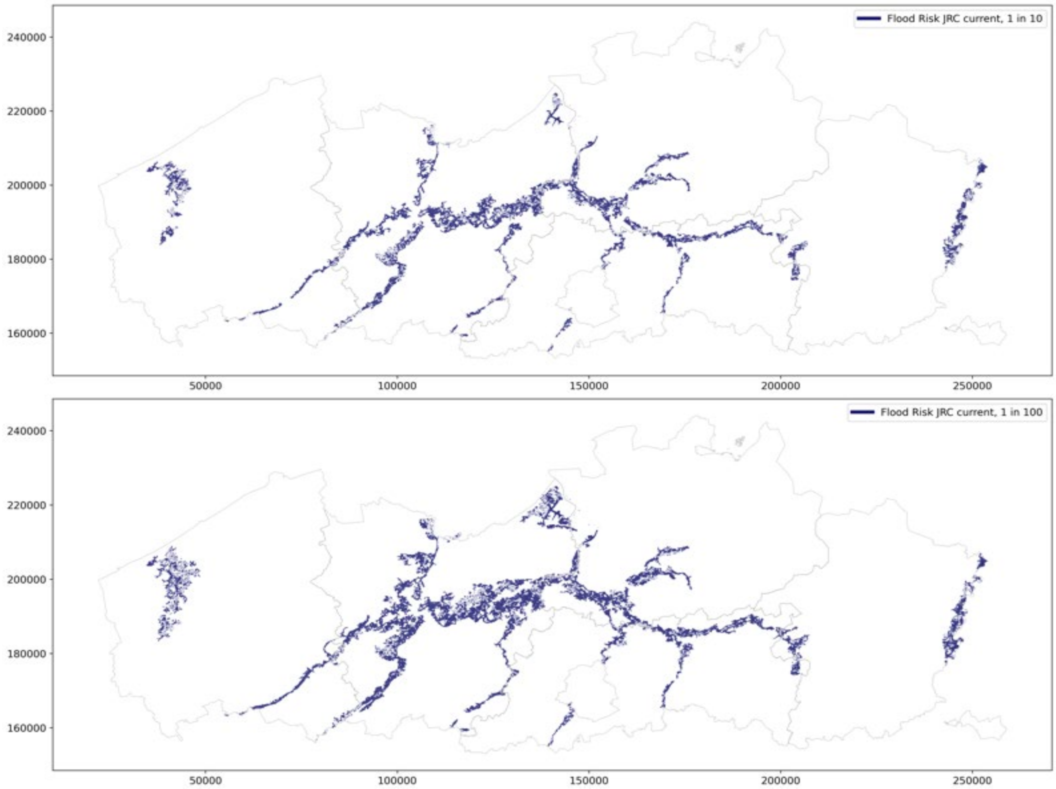

Figure 11: Comparison of JRC current flood hazard maps, 1 in 10 vs. 1 in 100.

We have already introduced the notion of return period/exceedance probability in section 1.3.1. However, an important note has to be made about interpreting it in this context. Here, a 10 year return period does not indicate that each year with ten percent probability, we would observe a comparable or worse flood as is depicted by the total flood hazard map in Figure 11. Intuitively this makes sense, since such a flood has never occurred in Flanders in the past. The return period here refers to the probability of observing a flood size equal to a single floodplain (polygon) instead of the full flood extent (all polygons). The probability of observing P1 (or worse) in Figure 10, for example, is 10%. This probability is equal across all polygons. The probability of observing all polygons (or worse) during a year is very low and unspecified by the JRC.

2.1.3 Underpinning choice EU-DEM and JRC flood maps

These two datasets were carefully selected. They both have some unique characteristics, making them the best choice for this application. The most significant advantage is that they provide cross-border data for all countries in Europe. This will prove very valuable when constructing future flood maps for the different European countries. However, the downside of using these cross border maps is their granularity. Especially the JRC maps' granularity is quite low. It only has a grid resolution of 100 meters. As explained in the previous section, this implies that the smallest flood the JRC is able to display is a square of 100 x 100 m. Compared to national maps, often providing an accuracy of 2 x 2 meters or higher, this is quite coarse. Undoubtedly, this limited granularity will limit the accuracy of the results. This is also indicated by Alfieri et al. who developed the JRC maps (2014). They explain that especially in small streams, the accuracy of the resulting extent and depth decreases significantly due to the difficulties in simulating extreme flood events. Also in steep valleys anomalously high water depths can sometimes be simulated. Fortunately, this problem is restricted to less than 0.001% of all flood hazard polygons. A more significant limitation of the JRC maps is that no flood protection or flood defenses are taken into account in the building process. Consequently, the resulting maps represent a worst-case scenario where the flood is such that all flood defenses fail. This assumption made by Alfieri et al. will be important to communicate to stakeholders when reporting on the final results.

Despite the previous limitations, these datasets are widely used by practitioners since regulators advise insurers to use these maps in climate-related analyses. In their opinion on the supervision of the use of climate change risk scenarios in ORSA, EIOPA states:

> *"How to assess the impact of physical risks (for floods) on a non-life insurance portfolio? In order to assess the potential impact that climate change could have on a non-life undertaking that covers flood risks, the Peseta IV study of the Commission's Joint Research Centre (JRC) on rising river flood risk in the EU could be used. (….) A non-life undertaking could*

> *use the study to (a) assess how much exposure it has in regions which are strongly impacted by rising river flood risk due to climate change, and (b) to estimate changes in insured losses on its underwriting portfolio due to climate change based on the projected change of overall economic losses under the different scenarios (Delcea et al., 2021, p.29)."*

EIOPA also distributed information to insurers on how best to incorporate climate change in the calculation of the solvency capital requirement (SCR) of natural catastrophes like floods. An SCR is the regulatory amount of capital an insurer has to hold to ensure that it can remain solvent throughout the year with 99.5% probability.[6] In their paper, EIOPA wrote that

> *"in order to integrate climate change aspects into the Nat Cat SCR calibration (…) EIOPA decided to rely mainly on the information from the European Environment Agency (EEA), the Peseta studies from the Joint Research Center (JRC) and the Intergovernmental Panel on Climate Change (IPCC) report (Delcea et al., 2020, p.5)."*

Next to EIOPA also regulators like the European Central Bank (ECB) suggest working with these flood maps when assessing financial stability (ECB, 2021). It is clear from these two examples that JRC maps benefit from a widespread regulatory support. Hence, choosing to work with them has a significant advantage. It facilitates the approval of results.

2.1.4 Data processing steps

Some data processing steps are necessary before being able to use the data. First of all, working with Geo-Spatial data, we have to be attentive to the coordinate reference system (CRS) used and make sure both data sets employ an identical one. Eurostat offers the possibility to download the DEM data in either a LAEA format with a unit in meters or a decimal degree (DD) format with a unit in degrees. However, the JRC maps can only be downloaded in a LAEA format.

Secondly, we have to calculate the elevation of the water surface with respect to sea level, since the JRC maps do not report on this value. From section 2.1.2, we know that the JRC polygons only have a depth attribute. This elevation of the water surface will be very important when building the forward looking flood maps later on in this chapter.

---

[6] For more background information on the SCR we recommend reading the regulatory text via https://www.eiopa.europa.eu/rulebook/solvency-ii/article-2324_en.

Figure 12 illustrates how we will derive it using the DEM. In this illustration we have a flood plain, P1, which lies between 2 hillsides next to the sea. P1 represents a single JRC flood polygon having a specific uniform $depth_{flood}$. To calculate the elevation of the flood surface, $Water\ level,$ illustrated by the orange arrow, we have to find the elevation of the surface beneath the flood, $elevation_{riverbed}$. This elevation is represented by the red arrow. It can be derived from the DEM, since the DEM represents a 3D view of the landscape. The DEM is visualized by the brown dots. We just select the DEM point at the bottom of the river. This is the red point.

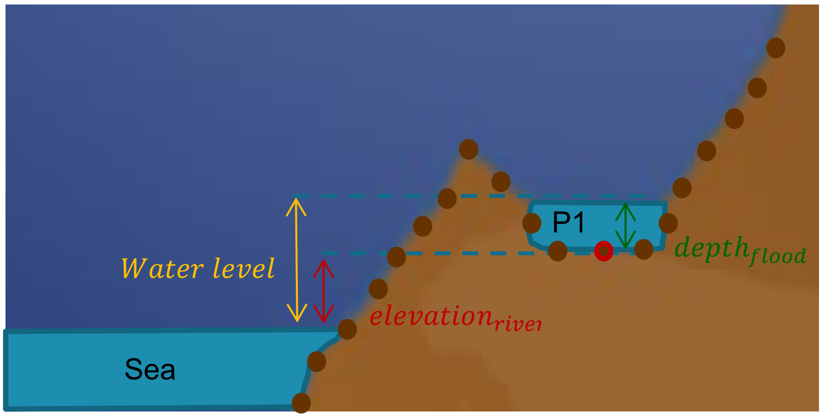

Figure 12: Illustration of the difference between the depth of the river (green arrow) which is relative to the surface beneath and the elevation of the water level with respect the sea level (orange arrow).

We then calculate the elevation of the water surface by:

$$Water\ level = elevation_{riverbed} + depth_{flood}.$$

(Equation 2)

We have used a simplified example to illustrate the method. However, choosing the red dot in practice is not straightforward due to the difference in granularity between the JRC polygons (100 m) and EU-DEM (25 m). Hence, in section 2.4.1, we will extensively comment on which problems occur and how we have tackled them.

2.2 A deep dive in the inner workings of the algorithm

The data is now in the correct format to construct forward-looking flood maps. This paper proposes a simple intersection technique. It is based on the interpolation method described in section 1.3.1 (Apel et al., 2009). However, we will not use it to construct a current flood hazard map. We will take a current JRC map as input and use the technique solely to make it forward looking.

Starting from a current map has some advantages. Firstly, the JRC map is constructed using complex hydrological and hydrodynamic models. Thanks to the results described in section 1.2.1, we know that most of the time this more complex method will yield more accurate results compared to using the interpolation method, especially when evaluating flat lowlands (e.g. Flanders). Secondly, it also allows us to leverage the information already contained in the maps, i.e., inundation depth and flood extent. This will prove very useful since, to make the current maps forward-looking, we must make assumptions on how climate change will affect floods.

In this paper we will assume that climate change will affect the inundation depth of the current flooded areas of the JRC maps. More specifically, the depth will increase (see green arrow in Figure 12) . In most countries, this is the expected evolution. However, in Czechia for example, scientists believe flood depth will decrease.[7] We will not run our algorithm on these countries since we can just take the current map as an upper bound for the future flood risk. This '*increase in flood depth*' assumption will have a large effect on the result. Hence, we will discuss it in length in section 2.4.2.

When the inundation depth increases, we expect the water to run further. Hence, the flood's extent will increase. This general idea is illustrated in Figure 13. As in Figure 12, P1 represents one specific JRC flood polygon having a uniform depth equal to the green arrow. However, due to climate change, the intensity of the flood swells. More specifically, in the future pane, P1's inundation depth increases by the purple arrow. We can illustrate this by P1 transforming into P2. At the same time, water will flow from this new polygon, P2, and fill up the empty areas to the left and right. This leads to P2's extent enlarging from the yellow line in the current pane to the black line in the future's pane.

[7] For more info see http://climate-impact-explorer.climateanalytics.org/

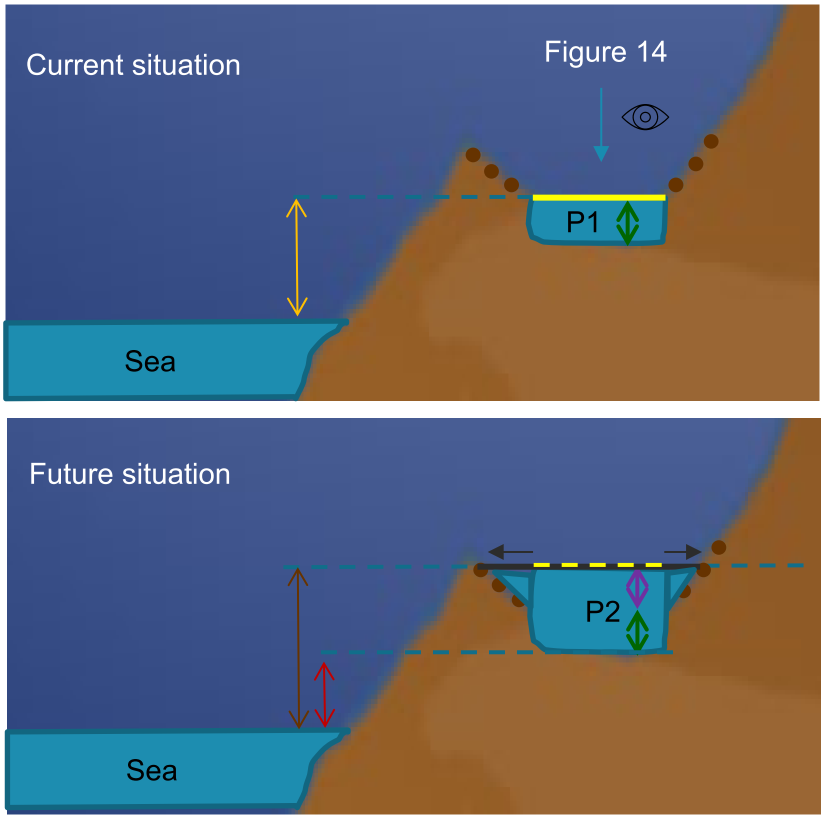

Figure 13: This figure illustrates what happens in the algorithm when the inundation depth of the flood (green arrow) increases by a certain amount (purple arrow).

This next part will detail how this general idea is applied by the algorithm to determine the flood's new extent (black line) after the increase in depth (purple arrow).

2.2.1 Set-up of the example: assumptions and intuition

We will use Figure 14 on the next page as an illustration to explain all the different assumptions and steps of the algorithm. Figure 14 consists of 90 blue JRC floodplains. It displays a birds eye view of a flooded area, similar to the one discussed in Figure 13 (side view). However the flood it describes is more realistic since it is comprised of more than 1 floodplain. Nonetheless, the intuition remains the same and we will regularly refer back to Figure 13 to illustrate the similarities.

To simplify the calculations, we assume that all 90 polygons have the same uniform depth of 3 meters. In Figure 13 this would mean that the green arrows of all flood polygons (only 1 displayed in Figure 13) have an equal length of 3 meters. Similarly, we also assume that the elevation of the surface below the flood polygons, represented by the red arrow in Figure 13, is always 6 meters. Hence, according to Equation 2, the elevation of all polygons water level is 9 meters since:

$$Water\ level_{current} = elevation_{riverbed} + depth_{flood}.$$

This elevation is represented by the orange arrow in Figure 13. In Figure 14, we have also depicted the surrounding DEM elevation points. To simplify the example, we only have 3 different elevations equal to 10, 13 or 14 meters. The darker the color the lower the elevation.

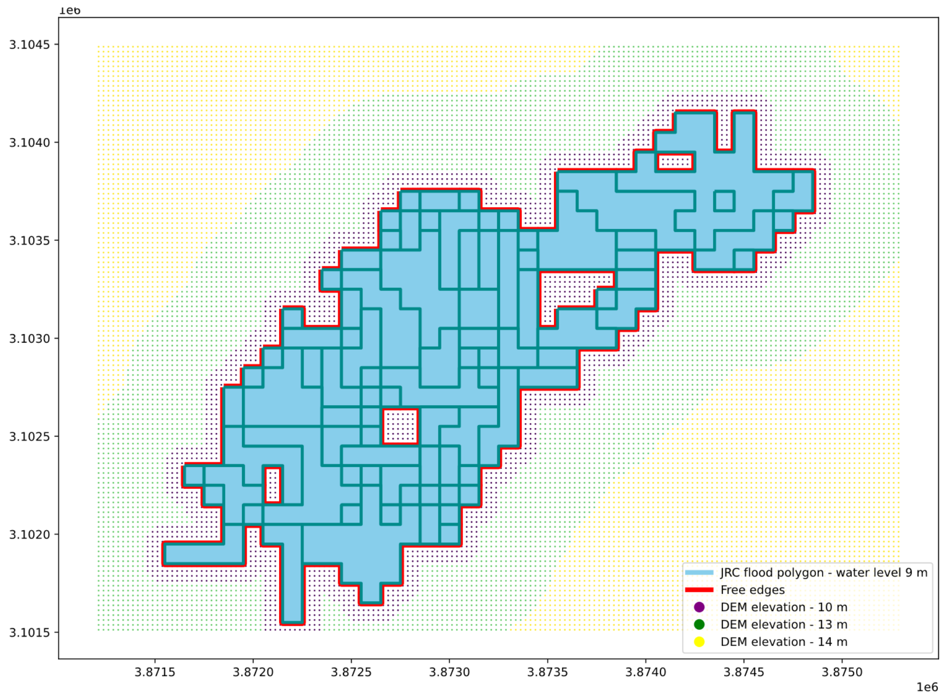

Figure 14 : Illustration of a flooded area comprised of 90 JRC polygons, surrounded by higher grounds. The red edge depicts the free edge that will be extended.

We assume that due to climate change the inundation depth will increase by 2 meters. Hence, the new water level, represented by the brown arrow in Figure 13 will be equal to 11 meters since,

$$Water\ level_{future} = Water\ level_{current} + Increase\ in\ depth.$$

After this increase in depth, we expect all DEM points which are below the $Water\ level_{future}$ to be flooded. In Figure 14, this would mean that all purple DEM points will lie in the future flooded area. Hence, we expect the extent to expand up to the green DEM points.

Before we can elaborate on the code itself, we will need to make some assumptions on how the water will expand when the depth in the original (blue) flooded area increases. We'll discuss them now before diving into the actual code.

2.2.1.1 Assumption 1: extend only the free edges

We first have to decide which are the appropriate edges to expand. This paper proposes to only extend the outer edges of the floodplains. These are depicted red in Figure 14. The reason why we only extend these edges is that we want to efficiently calculate how the current flood prone area will increase. Fortunately, extending only the outer edges will not lead to loss of information.

The reason is visualized in Figure 15. We have 2 JRC polygons, A and B, representing a current flooded area. After an increase of their depth (purple arrow), we expect the flood's extent to increase. Intuitively, we expect that the new flood will stop at the black points. The red arrows illustrate the extension of the outer edges. We indeed find the points we expected. Extending the inner edges would also lead to the same points. This is illustrated in yellow. Hence, they do not add information. Evaluating them would only lead to a significant increase in the runtime of our algorithm.

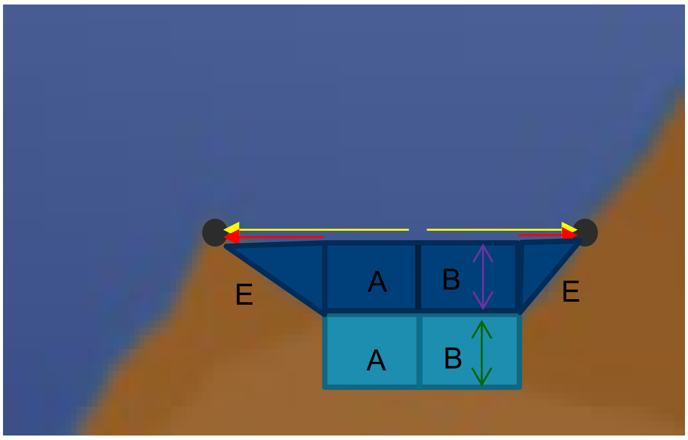

Figure 15: Illustration of the extension of the flooded areas A and B after an increase of the inundation depth (purple). The extension E of the outer (red) and inner (yellow) edges both lead to the same point.

2.2.1.2 Assumption 2: Extend the free edges perpendicularly

The second assumption concerns the flood direction. Figure 16, which is a zoomed image of the top left corner of Figure 14, visualizes two options. We will investigate what happens when expanding edge E1 and E2 in both cases.

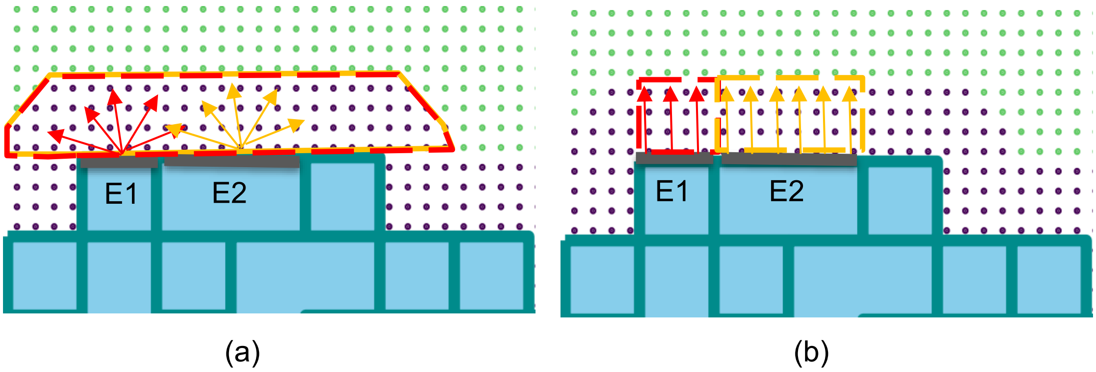

Figure 16: Illustration of 2 different flood dynamics. Pane (a) assumes water can flow freely in all directions, while pane (b) restricts water to only flow perpendicular to the edge.

Option a represents the most realistic scenario where water is flowing in all free directions, as indicated by the arrows. The resulting flood due to expanding edge E1 is plotted in red while the expansion of E2 is plotted in orange. We notice that both extensions overlap. Option b restricts the flow of water to happen only perpendicular to the edge. It is a simplification with respect to the more realistic view of water flowing freely in all directions. We now see that the extensions are adjacent but do not overlap anymore.

This paper proposes to extend the edges perpendicularly since it will speed up the runtime of the algorithm. This is mainly because when extending a polygon's edge, we only have to evaluate the perpendicular points instead of all points. Evidently, this will result in some loss of information. However, we believe that the positive effect on efficiency outweighs the rather small effects on accuracy, since the main goal of this algorithm is to evaluate very large areas efficiently.

2.2.1.3 Assumption 3: Extend the free edges in a discrete way

The last assumption again simplifies with respect to reality in favor of runtime efficiency of the algorithm. We will assume that the edge is not extended in a continuous way. Instead, we opt for a discrete approach where each free edge is divided in equally spaced points, 25 meters apart. To illustrate this we have discretized the edge E1 indicated with black points in Figure 17. Each separate point is then perpendicularly extended, following the approach explained in the previous subsection. In red we have indicated those points which would make up the new flood extent.

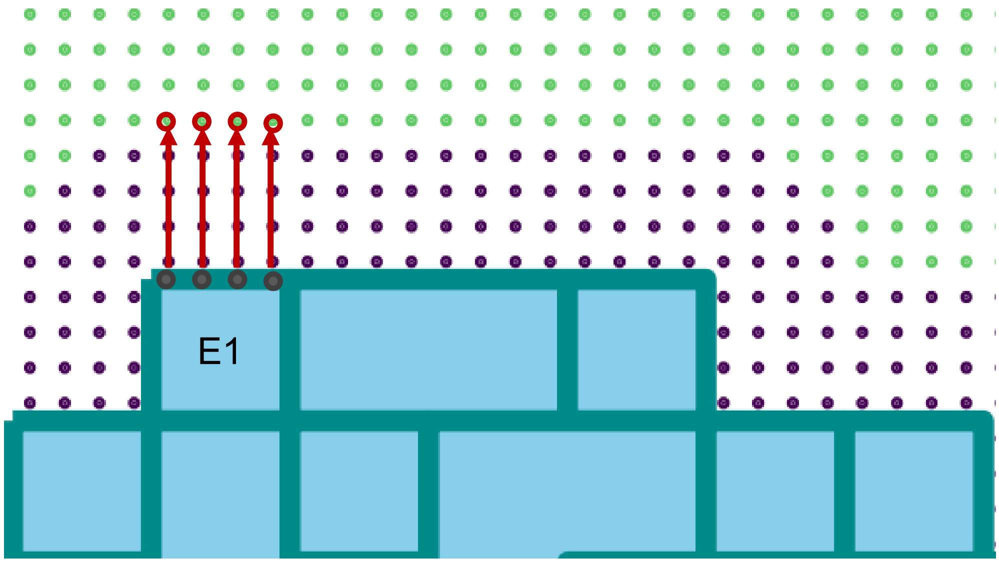

Figure 17: An illustration of a free edge divided in equally spaced points in black. After extending perpendicularly, the red points are returned as points to make up the new extent.

It would be possible to soften this assumption by letting the points be closer to each other. In theory, this should lead to more granular results. However, in practice this is not the case due to the specific granularities of the DEM and JRC map. The idea is visualized below in Figure 18. Since the DEM is set up as a grid of points spaced 25 meters from each other, the same DEM points will be returned by the algorithm when decreasing the spacing to e.g. 12.5 m. Hence, evaluating those points would only lead to a drop in runtime efficiency of our algorithm.

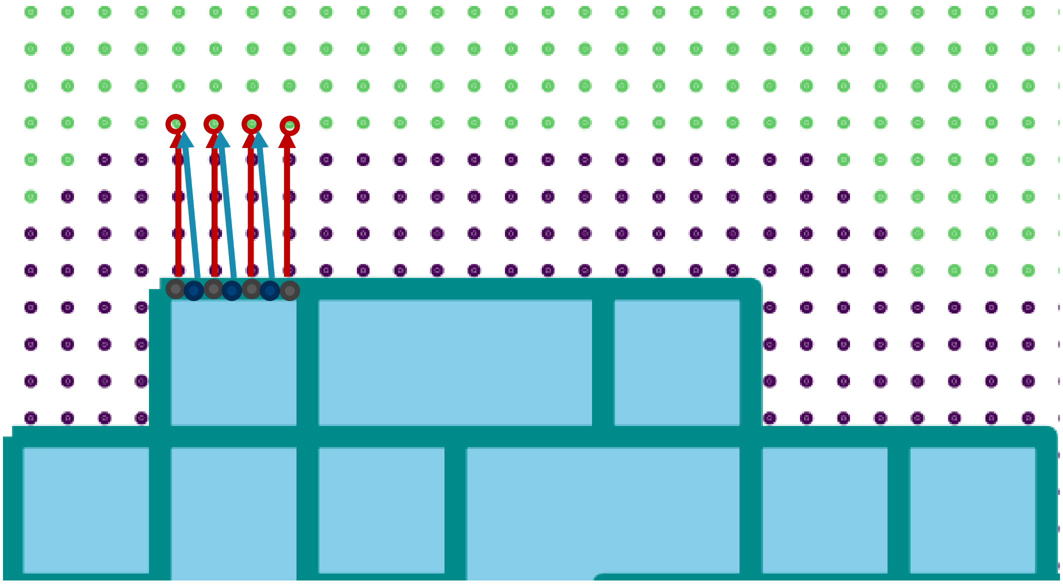

Figure 18: This figure illustrates that dividing the free edge in more points will not lead to more accurate results. It will only slow down the algorithm.

Using the previous examples and the explanation of the different assumptions, we will now elaborate on all steps of the algorithm. These steps are visualized in pseudocode in the next subsection. In this code, we loop over all polygons in the JRC map, evaluating them separately. However, we will pick one polygon to illustrate the steps. This polygon, P1, is visualized in the next figures in dark blue. This paper has used Python to implement the code. Python is a good choice for this purpose since Python packages like Shapely, Geopandas and Scipy allow for easy processing of geospatial data.

2.2.2 Algorithm applied to the example

Step 1: Find the free edges

for *t=1,…,T* **do**

Find all neighbors of $polygon_t$ i.e. all polygon sharing an edge with $polygon_t$;

Calculate the S free edges of $polygon_t$ having no neighbor;

Step 2: Discretize outer edge

for *s=1,…,S* **do**

Divide $edge_s$ in V equally spaced points 25 meters apart:

Step 3: Filter DEM

for *v=1,…, V* **do**

Calculate $Water\ level_{new,v} = water\ level_{old,v} + Increase\ in\ depth$;

Filter out all points in EU-DEM below $Water\ level_{new,v}$;

Find closest point perpendicular to free edge in filtered EU-DEM;

Step 4: Find edge of new extent

Connect found points linearly such that it becomes the extended edge;

Connect extended edge with free $edge_s$ by perpendicular lines;

Algorithm 1: Building a future flood map.

2.2.2.1 Step 1: Find the free edges

The first step in the algorithm selects the free edges to expand. Based on assumption 1, we know that these are the outer edges, depicted red in Figure 14. To find these in practice, the algorithm first selects all neighbors of P1. These are displayed yellow in Figure 19.

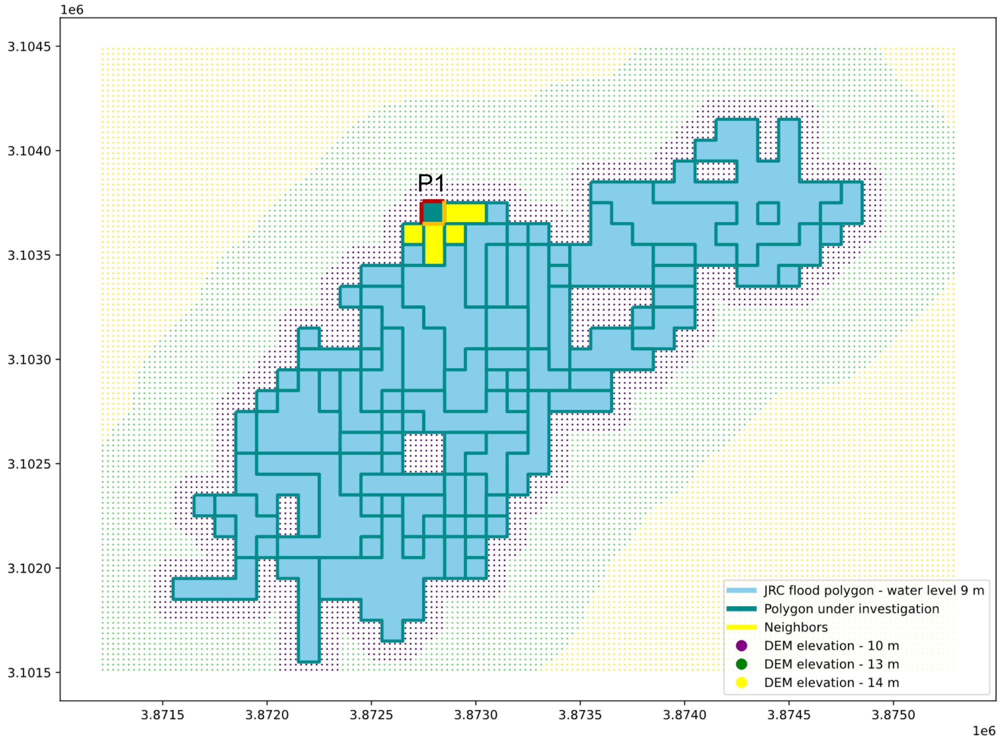

Figure 19: Illustration of P1's neighboring polygons.

These neighbors can be found by looping over the whole JRC dataset and returning all those polygons which are adjacent to P1. To find the free edge, we then take the difference between P1's edge and the edges of the neighbors. Hence the orange part of P1's edge is deleted. We end up with the red free edges.

2.2.2.2 Step 2: Discretize outer edge

The second step discretizes the edge. It does this by splitting it up in equally spaced points, 25 meters apart. Figure 20 visualizes this step. It is a zoomed image of P1 in Figure 19. The black dots represent the discretized outer edge.

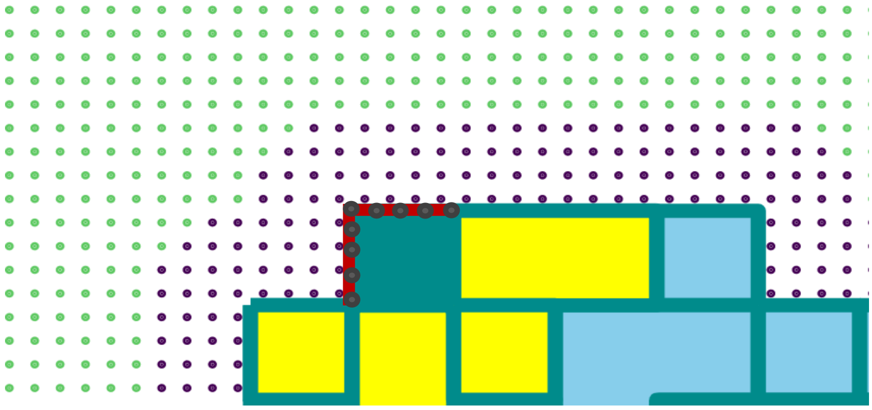

Figure 20: Discretization of the outer edge.

2.2.2.3 Step 3: Filter DEM

We are now ready to extend each point separately, perpendicular to the edge. This is done by an intersection technique. This technique starts by filtering the DEM such that only those points with an elevation higher than the new water level remain. All other points are flooded. From the set-up in section 2.2.1, we know that the new water level is 11 meters. Hence, since the purple DEM points have an elevation of 10 meters, they will be filtered out. The resulting DEM can be consulted below.

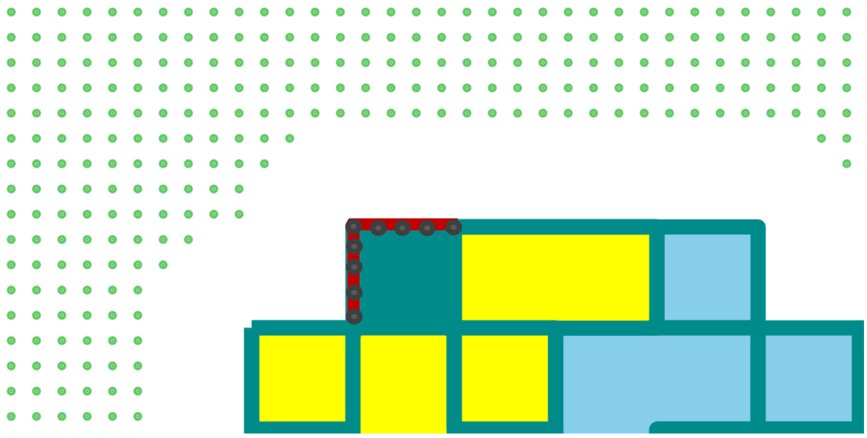

Figure 21: The resulting DEM points after filtering out the flooded points (purple DEM points).

2.2.2.4 Step 4: Find edge of new extent

The final step determines the new extent. It does this by intersecting perpendicular lines, starting at each of the discretized points, with the remaining DEM points. This process is visualized in Figure 22 by the black lines. The intersections in grey, denote the first points in the landscape not flooded due to the increase in depth.

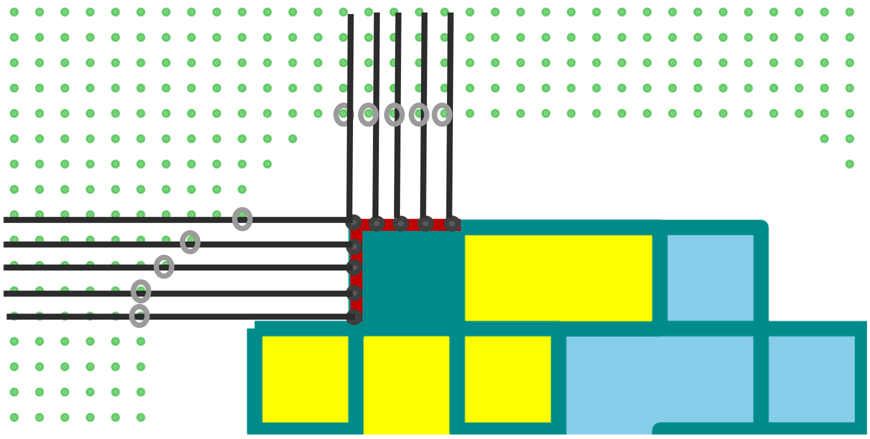

Figure 22: : Intersecting the DEM to find the future flood extent.

By linearly connecting all black and grey points, we find the new flood extents, E1 and E2. These have been plotted in Figure 23. In theory, these extensions should always have sides perpendicular to the original edge. However, due to granularity differences between the DEM and JRC, they could be slightly skewed. This is, for example, the case for extension E2.

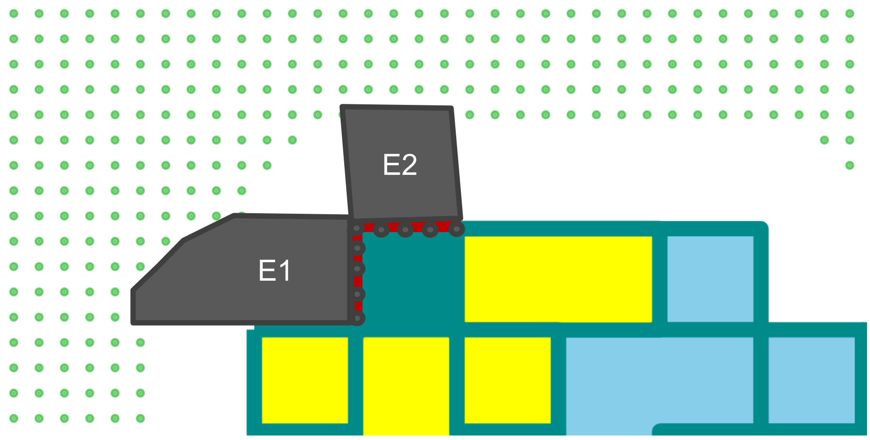

Figure 23: E1 and E2 are the extended edges after an increase of the inundation depth of 2 meters.

After this step, the algorithm selects the next polygon and repeats the process. The total extension can be consulted in Figure 24. It is clear that in this simplified example the algorithm performs quite well, flooding almost all areas which should be flooded.

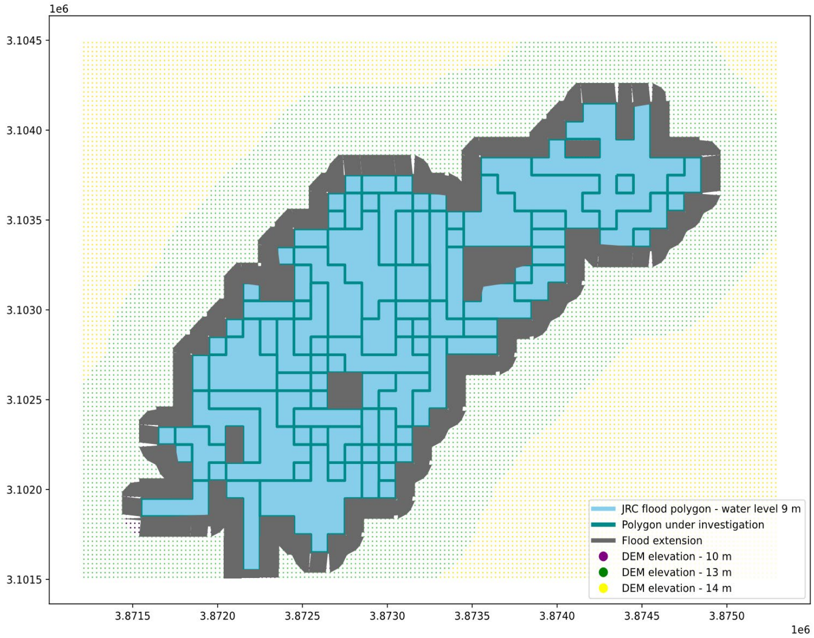

Figure 24: Extension of all free edges, depicted in black.

2.3 How well does the algorithm perform?

This section evaluates the previously detailed algorithm. To better illustrate the potential pitfalls and flaws, we will relax the assumption that only 3 different DEM elevations exist. This will lead to a significantly more challenging terrain to run our algorithm on, making it harder for the algorithm to capture all relevant areas. Figure 25 represents the new area.

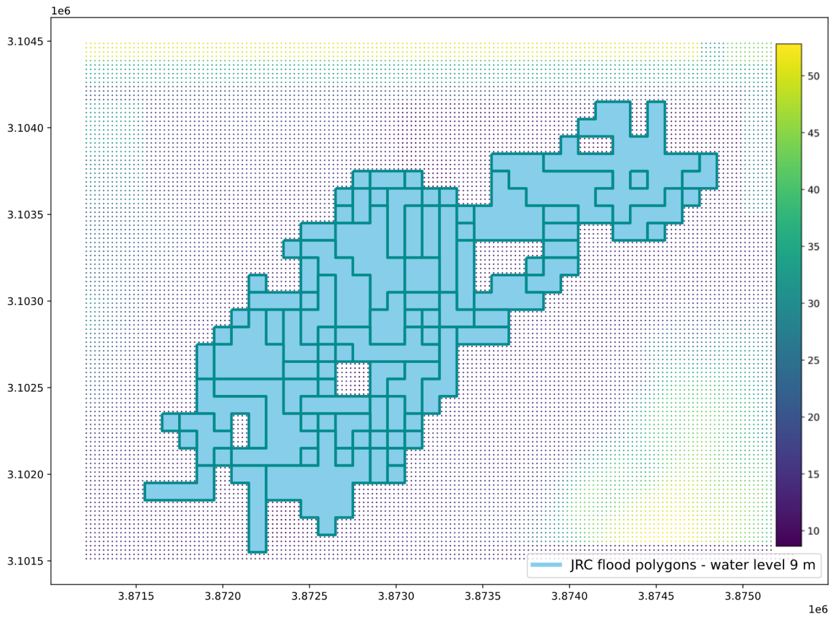

Figure 25: An illustration of a JRC flooded area, consisting of 90 blue polygons, located in a non-uniform landscape.

Like in section 2.2, the blue polygons are floodplains and represent the current flooded area. They have a uniform water depth of three meters and a water level of nine meters. The elevation of the surface below the water is thus six meters. The dots illustrate the elevation points in the EU-DEM. Darker points represent lower elevations. Lighter colors represent a more elevated landscape. Figure 26 differs from Figure 25, as all the elevation points below 11 meters are filtered out. The resulting white space should be flooded as much as possible by our algorithm after an increase of the water level by two meters.

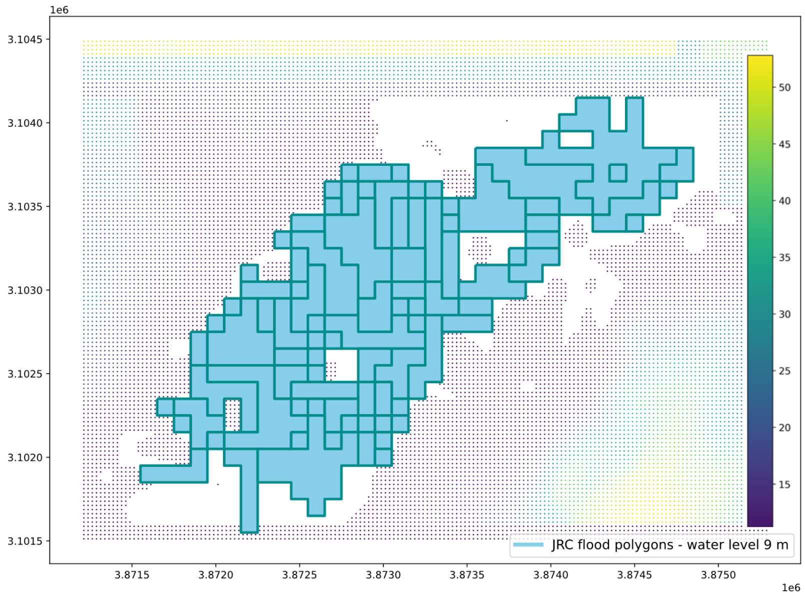

Figure 26: All elevation points below 11 m have been filtered out of the DEM, since these points should be flooded after a 2 m depth increase.

Figure 27 shows the resulting future flood map after the inundation depth increased by 2 meters.

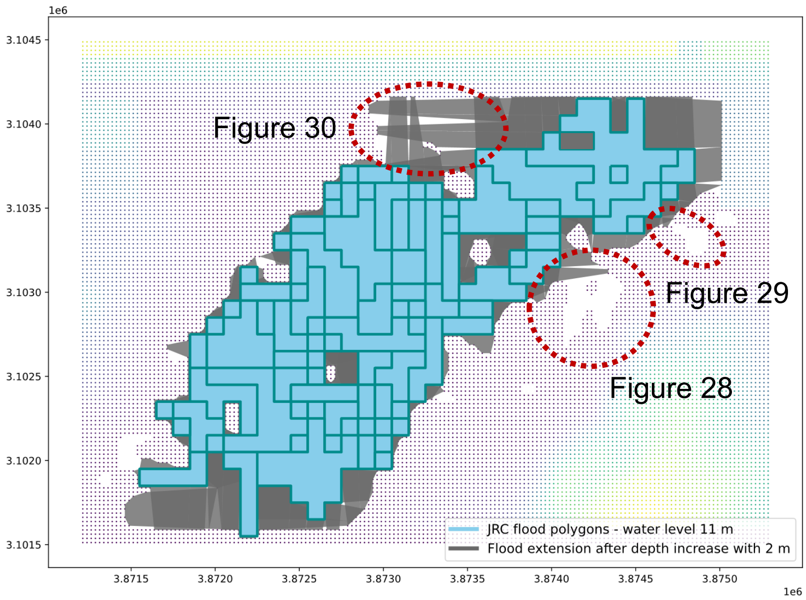

Figure 27: The blue and black areas depict a future flooded area after an increase of the depth by 2 meters.

We will now discuss this future flood map extensively, describing the weaknesses and areas which need further research. We will also further elaborate on some of the assumptions made.

2.3.1 Not capturing all relevant areas

We have chosen a quite challenging terrain to run our algorithm on. However, especially in the interior, it does a good job in flooding most areas which are below the new water level. Also, outside of the current flooded area, the program is able to follow the outlines of the elevated terrain quite accurately. However, some areas, which intuitively should be flooded, are not fully captured. This underestimation of the total flood is mainly due to some of the assumptions we made in combination with the simplicity of our intersection approach. We have highlighted the general location of the problem areas in red on Figure 27. We will now zoom in on each of these and discuss them.

The first location the algorithm struggles to correctly flood is displayed in Figure 28. Here, lower grounds, i.e., terrain with an elevation below 11 meters, takes a turn and is shielded by some higher grounds. Since the algorithm limits the flood to happen only perpendicular to the edge of the polygons, the extensions are not able to capture this area. This leads to an underestimation of the flood.

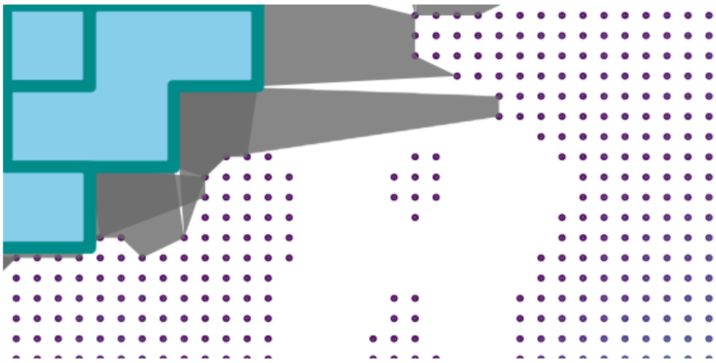

Figure 28: Underestimation of the flood due to a turn in the lower grounds of the terrain.

Also, lowland past a neck of land will not always be captured. An illustration of such a terrain can be consulted below in Figure 29. This underestimation happens due to the simplicity of the intersection technique. It is not able to recognize the small neck of land through which water should flow.

Figure 29: Underestimation of the flood due to a neck of land.

Also in the north west corner of Figure 27, not all areas are flooded. This is induced due to the little islands of higher grounds shielding lower lying areas at the other side. We have encircled such areas in Figure 30.

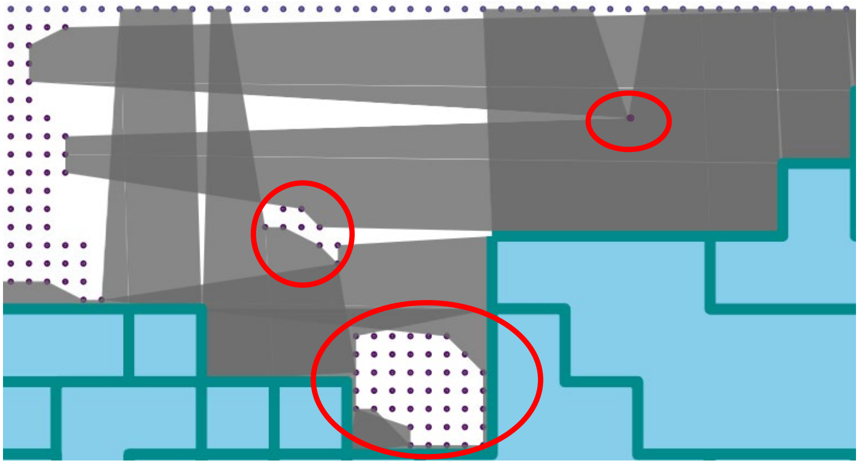

Figure 30: Underestimation of the flood due to groups of higher elevation points shielding lower areas.

These three problems occur especially in flat lowland and mountainous regions and thus will limit the accuracy of the results, as was indicated by Apel et al. (2009) in section 1.3.1. To solve these issues, this paper suggest a small adaptation of the algorithm.

Instead of calculating only the extensions of the current flooded area, the algorithm will now also perpendicularly extend the edges of the black polygons. Figure 31 illustrates this idea by extending E1. The new extension, E2, almost captures the whole problem area. By iteratively extending the edges, the algorithm is able to capture a turn in the terrain (Figure 28). This adaptation would also help in capturing lower grounds beyond neck of lands (Figure 29) and groups of higher elevation points (Figure 30).

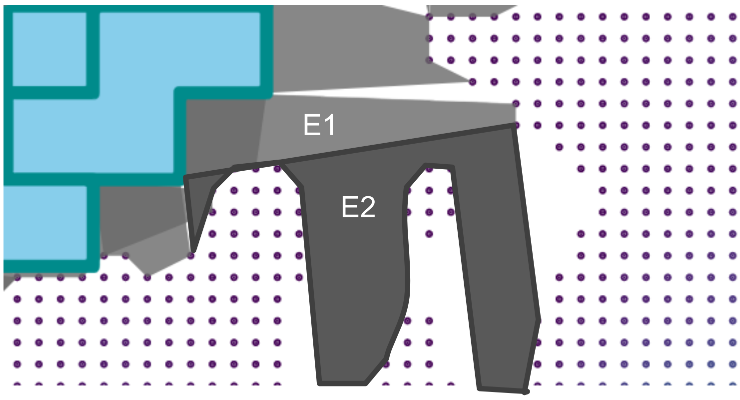

Figure 31: Extending the extension E1 results in the extension E2 which already captures most of the problem area.

A downside of this adaptation is that it will have a large impact on the runtime of the algorithm. If we start with 5.000 polygons then, on average, we end up with more than double the amount of extensions. If we iteratively keep extending the extensions, the amount of edges to evaluate would increase exponentially. Moreover, in this area, the increased accuracy could justify the longer runtime. However, in many other areas, behaving like the southern and western part of Figure 27, it would not lead to any better predictions. It would only affect the runtime. Hence, since time and computational power are limited in a company context, we decided to not implement this additional step. Some more research should be conducted to efficiently capture all problem areas.

2.3.2 Runtime

The algorithm depends extensively on the filtering of DEM datasets. When evaluating small areas, this filtering has a minimal effect on the performance, evaluating +-3 JRC polygons per second. However, when expanding the area, the runtime explodes. Tests reveal that the most computationally expensive step occurs when filtering out all DEM points below the new water level. This drop in performance is due to the elevation dataset, that becomes massive fast for larger regions. When assessing an area, the extent of Flanders, the algorithm slows down to evaluating 1 JRC polygon per 15 seconds. Calculating Flanders' forward-looking flood map would then take more than three days.

To speed up this approach, one could try to split up the DEM in N nonoverlapping frames, F. In mathematical notation this translates to:

$$DEM = \bigcup_{i=1}^{N} F_i \quad s.t. \quad F_i \cap F_j = \emptyset \qquad \forall\, i \neq j,\ with\ \ i,j = 1, \dots N.$$

We would then assign each polygon to the DEM frame, F_i, it belongs to and filter only in that data frame. However, this technique has a significant drawback that is illustrated in Figure 32. We see that polygon P is situated quite close to the blue dashed edge of its frame F_1. Consequently, when extending segments of its red free edge to the right, no elevation points that are higher than the water level will be found, since the first points higher are situated in the neighboring frame F_2. This will distort the results.

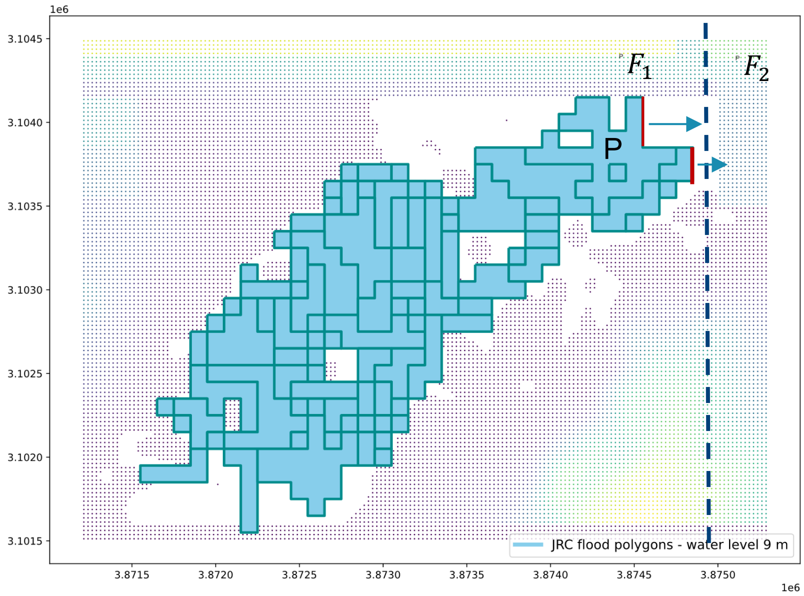

Figure 32: This figure illustrates that splitting up the DEM in nonoverlapping frames could lead to errors whenever polygons are locate to close to the frame's edge.

To solve this issue, we propose a novel rolling window inspired procedure. The difference with the previous approach is that we now ensure that neighboring frames, like F_1 *and* F_2 overlap. Hence, we soften the condition of no overlap such that:

$$DEM = \bigcup_{i=1}^{N} F_i \quad s.t.$$

$$F_i \cap F_j = \emptyset \qquad \forall\,(i \vee i+1) \neq j \;\; with \;\; i,j = 1, \dots N-1,$$

$$and$$

$$F_i \bigcap F_{i+1} \neq \emptyset \; with \; i = 1, \dots, N-1.$$

After this step we again assign the polygons. Each polygon is assigned to the frame it belongs. Whenever a polygon is situated in a coinciding area, it is assigned to the frame whose edge is the furthest. If the polygon is precisely in the middle, the most left frame is assigned. Figure 33 illustrates the new situation. Contrary to the situation above, P is now assigned to F_2 since F_2's green frame's edge is the furthest away. Consequently, all red free edges can be extended without problems. Hence, we have solved the problem, while maintaining the runtime efficiency.

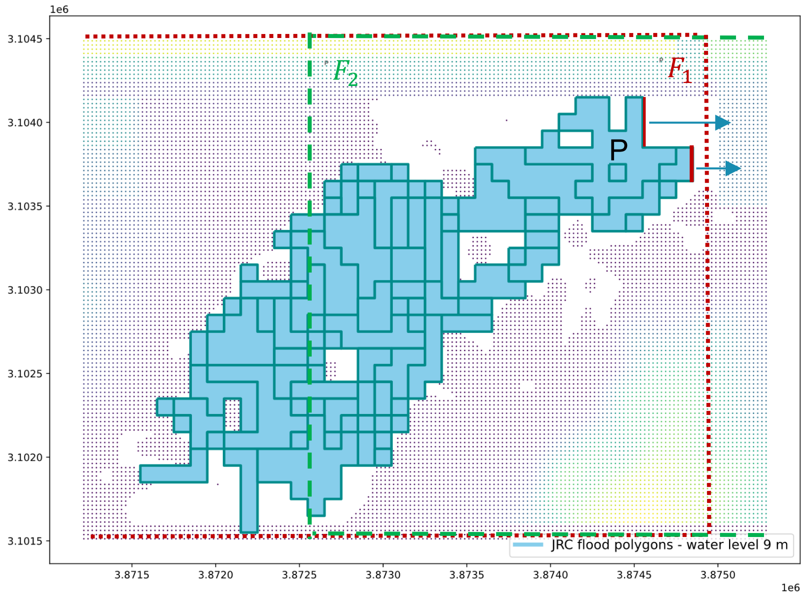

Figure 33: Overlapping the DEM frames ensures that enough DEM points are always present to be able to extent the edges.

2.4 Assumptions made in the algorithm

The accuracy of the algorithm depends significantly on some of the assumptions made. Hence, we will discuss them in some more depth. We will first elaborate on the estimate of the water surface elevation. Next, we will zoom in on the '*increase in depth*' assumption.

2.4.1 Calculating the elevation of the water surface relative to sea level

In section 2.1.4, we explained how we can use the DEM to calculate the elevation of the JRC water surface with respect to sea level as

$$Water\ level = elevation_{riverbed} + depth_{flood},$$

where $depth_{flood}$ is an attribute of the JRC polygons. We also mentioned that in practice choosing the correct $elevation_{river}$ from the DEM is not straightforward and multiple options exist. However, we did yet not elaborate on the issue. Since the algorithm depends significantly on the use of $Water\ level$, choosing one of the possible $elevation_{river}$ is an important assumption. Hence, we will detail it in the next paragraphs.

The problem links directly to the difference in granularity between the JRC polygons (100 m) and the EU-DEM (25 m). Due to this difference, each JRC polygon contains at all times, at least 16 different elevation points. Figure 34 illustrates the smallest possible JRC polygon, i.e., a square with sides of 100 m, having a $depth_{flood}$ of 1 meter. We can clearly see that 16 elevation points are encompassed by the polygon. All these are candidates to be used as proxy for $elevation_{river}$ in the calculation of $Water\ level$.

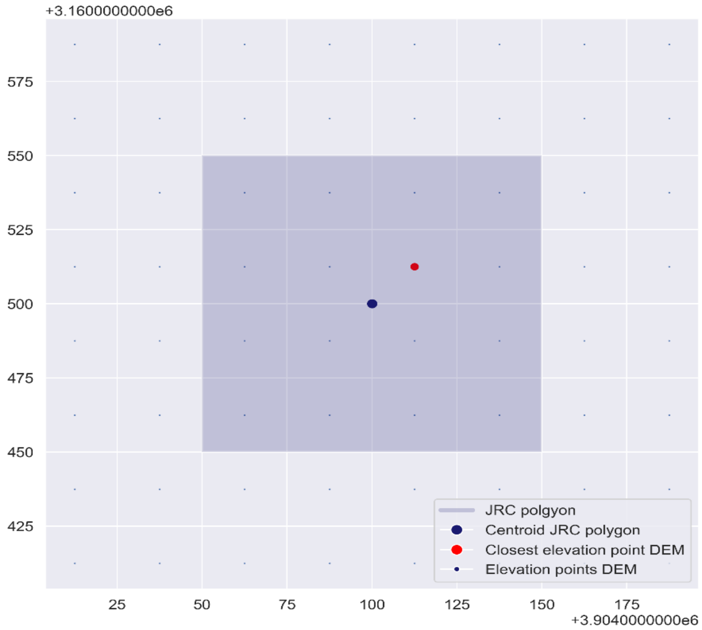

Figure 34: Illustration of the smallest JRC polygon and the surrounding elevation points.

Table 3 lists, for the polygon illustrated in Figure 34, all possible $Water\ level$ values, calculated using the different $elevation_{river}$ DEM points and a $depth_{flood}$ of 1 meter. We clearly observe a lot of dispersion between the different possibilities, which range from 0.17 to 2 meters. The corresponding standard deviation is 0.6 meters.

Index	Geometry	Elevation (m)	Water level (m)
1	POINT (3904062,5 3160537,5)	1,0094495	2,0094495
2	POINT (3904087,5 3160537,5)	0,36984685	1,36984685
3	POINT (3904112,5 3160537,5)	-0,3942439	0,6057561
4	POINT (3904137,5 3160537,5)	-0,8043613	0,1956387
5	POINT (3904062,5 3160512,5)	0,7273291	1,7273291
6	POINT (3904087,5 3160512,5)	0,17002274	1,17002274
7	POINT (3904112,5 3160512,5)	-0,48873723	0,51126277
8	POINT (3904137,5 3160512,5)	-0,81988466	0,18011534
9	POINT (3904062,5 3160487,5)	0,4160358	1,14160358
10	POINT (3904087,5 3160487,5)	-0,05325962	0,946474038
11	POINT (3904112,5 3160487,5)	-0,5838722	0,4161278
12	POINT (3904137,5 3160487,5)	-0,8271624	0,1728376
13	POINT (3904062,5 3160462,5)	0,12432925	1,12432925
14	POINT (3904087,5 3160462,5)	-0,24123898	0,75876102
15	POINT (3904112,5 3160462,5)	-0,6634406	0,3365594
16	POINT (3904137,5 3160462,5)	-0,8296623	0,1703377

Table 3: An extract of the DEM dataset (Copernicus program, 2016). We selected all those elevation points lying in the square polygon of Figure 36 and calculated what their water level would be depending on which DEM elevation point is selected.

The question is now, when extending a certain edge, which water level should the algorithm pick. Due to the coarseness of the JRC maps and the corresponding variance in water levels, choosing a wrong one could have a significant impact on the accuracy of the extension. Should we use the elevation point closest to the centroid of the polygon, indicated in red in Figure 34, or should the algorithm, for example, pick the DEM elevation closest to the point it tries to extend?

There is no clear answer. However, this paper decided to simply use the centroid of the polygon. We based this decision on Alfieri et al. (2014) giving an indication of what we should do. In their paper, describing the methodology of the JRC maps, they say that "simulation domains were assigned a square shape, so that the river pixel where the input flood hydrograph is introduced lies in the centre of each domain" (2014). For that reason, we chose the centroid of the polygon. However, this is an area in which the algorithm, as proposed in this paper, could benefit from further research.

2.4.2 Increase in inundation depth due to climate change

In this section we will comment on the second important assumption made by the algorithm, i.e. the increase in inundation depth. This parameter captures how climate change will affect the average depth of a flood through time. It is used by the algorithm as input when filtering the elevation dataset and is thus key to building a realistic flood extent map.

To ensure the reliability of the results, we must obtain a proper estimation of the increase in inundation depth. Preferably, this estimation can be linked to a climate framework, such as the NGFS discussed in section 1.2. This makes it easier to report on the assumption to regulators. It also enhances credibility of results.

However, deducting it from data is not a straightforward exercise, as to our knowledge no granular dataset is freely available providing the information needed. Fortunately, the climate explorer tool from the NGO Climate Analytics offers a publicly available solution.

The climate impact explorer website from the NGO Climate Analytics offers a wide variety of tools and papers related to climate change. The organization was founded in 2008 to guide policy makers and governments in adopting their climate change strategies. It is supported by a wide variety of universities and well-regarded institutes like the Joint Research Committee. Also regulators like EIOPA advise using the tools when performing climate risk related analyses. In the follow-up document on their 'Opinion of the use of climate change risk scenarios in ORSA' (Delcea, 2021) of April 2021, where EIOPA gives some practical guidelines on how to perform climate analyses, the climate tool is used (EIOPA, 2021). This approval by EIOPA is a major asset to an insurer, when deciding to use the tool in its own analyses, since it can facilitate significantly the approval of the results. Something which often is not very straightforward.

Moreover, this tool provides data on how flood depth will increase through time. Additionally, it also distinguishes between the different NGFS scenarios. It thus provides data on how flood depth will increase in each climate pathway. Hence, it contains all the necessary information for us to underpin the increase in depth assumption on which the accuracy of our future flood maps heavily rely. Furthermore, these changes in flood depth are also reported for a lot of countries separately. Therefore, this tool will be key to build country specific future flood maps for each NGFS climate pathway and time horizon. Figure 35 gives an example of how the tool looks like. It shows how flood depth is expected to evolve in Belgium under two different NGFS scenarios.

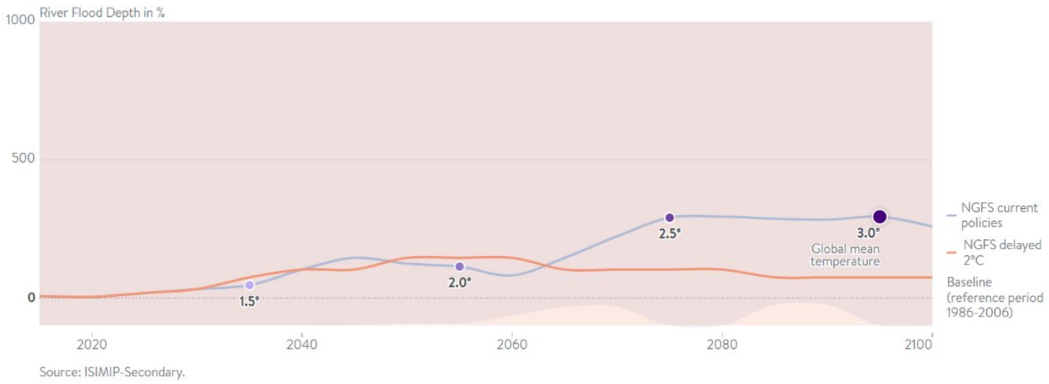

Figure 35: Flood depth evolution in Belgium under the NGFS current policies and delayed transition scenarios, from http://climate-impact-explorer.climateanalytics.org/.

3 Comparing flood risk models: white box vs black box

In chapter 1, we defined all the essential elements needed to understand and perform a flood risk analysis. We discovered that accurate current and future flood maps are key to the success of such an analysis. However, this paper also pointed out that future flood maps are often not publicly available outside Flanders. Hence, in chapter 2 we developed an algorithm to derive future flood maps from free to use governmental data. We called these maps the JRC extended maps. This chapter now proposes a white box model which relies solely on publicly available data and the extended maps. Hence, it does not require any input from brokers or local governments. The goal is to assess how prone an insurer is to floods.

To assess how well our model compares to the industry standard, we will first explain in some more depth how a flood risk assessment is often performed by practitioners when using a black box broker tool. This will be the base case used for comparison with our own developed model. We will explain how the hazard, exposure and vulnerability components, as set out in chapter 1, are modeled. We will define the same elements for the white box model to facilitate the comparison.

We have chosen Flanders as a use case to illustrate the model since the Flemish government is one of the only governments in Europe to provide both current and future flood maps.

3.1 A black box broker model approach

3.1.1 Hazard: VMM maps

The hazard is modeled by the official flood maps provided by the Flemish government (Vlaamse Milieu Maatschappij, 2021). We will refer to them as the VMM maps. Both current and future maps, taking into account a climatological projection of 30 years, are available. These hazard maps give a very granular view (~2m resolution) on the flood extent and depth for different scenarios. The maps are present for one in 10, 100, and 1000 year return periods (RP). An example of both current and future 10 year maps can be found in Figure 36. Visually, this map shows us which locations in Flanders are at risk of being flooded according to the Flemish government. The areas currently at risk are colored light blue. This represents the current flood map. The areas which become at risk, due to climate change by 2050 are colored dark blue. Hence, this is the future flood map.

Comparing both gives us some intuition on the effects of climate change on flood risk.

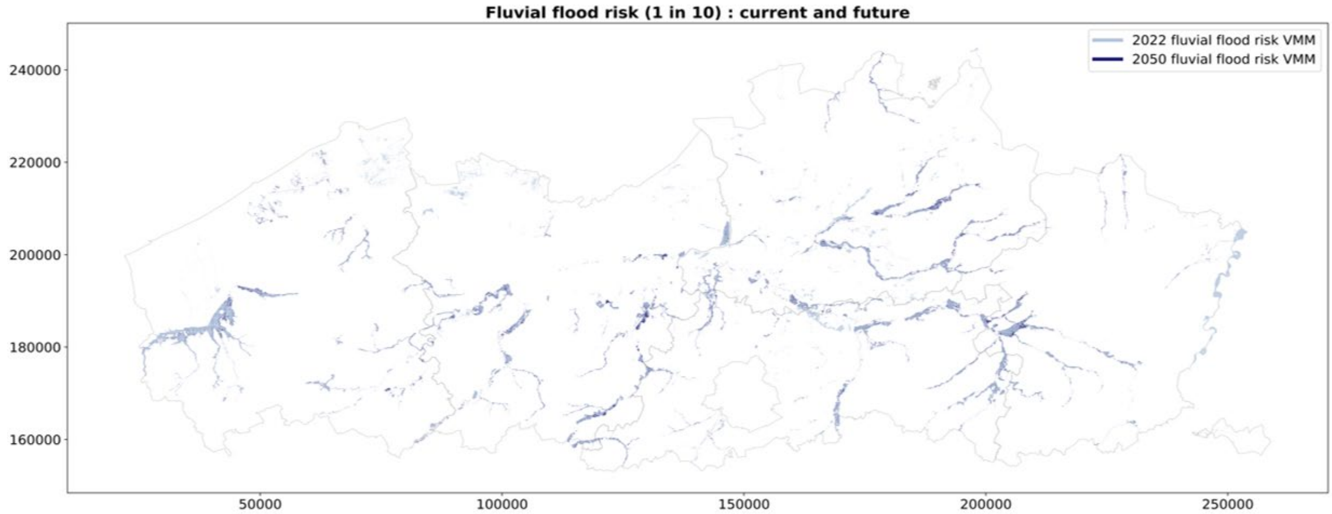

Figure 36: 10 year fluvial flood risk exposure in Flanders as provided by the VMM.

3.1.2 Exposure

In the introduction of this paper we explained that, in Belgium, fire insurance covers the material damages of floods. Hence, to proxy an insurer's exposure, which are the buildings and objects covered for flood (Kron, 2005), we can use its fire insurance portfolio. However, not all policies in this portfolio are at risk of suffering damages according to the VMM flood hazard maps. Only those located in the flooded areas could suffer losses. Hence, to derive an accurate estimate of the exposure, we select only those properties located in the at-risk areas and add their sum insureds to get an estimate of the flood exposure under the VMM maps. Suppose that n_1 buildings are at risk in the current map with 10 year RP and n_2 buildings in the future map with same RP, we can calculate the exposure as:

$$VMM\ exposure_{current,10} = \sum_{i=1}^{n_1} sum\ insured_i$$

and

$$VMM\ exposure_{future,10} = \sum_{i=1}^{n_2} sum\ insured_i,$$

(Equation 3)

where $sum\ insured_i$ is the sum insured of building i. Note that maps with higher RPs will have more flood exposure, i.e. more buildings at risk, since they represent more severe flood scenarios.

Equation 3 represent the total sum insured at risk for flooding. If a flood destroys all n_1 at-risk buildings this year, $VMM\ exposure_{current,RP}$ is the claim amount the insurer expects to receive. However, this is not a realistic scenario. To transform this total flood exposure into a more realistic expected flood claim, we model the vulnerability. As explained in section 1.3.3, this component captures how vulnerable the assets are in case of flooding (Kron, 2005).

3.1.3 Vulnerability: broker factor

In the introduction of this paper, we mentioned that insurers often rely on proprietary broker tools, like Q-FLAT from Aon or G-CAT from Guy Carpenter, to model flood risk. The disadvantage of this approach is that an insurer cannot always get sufficient actionable insights from these tools since only end results are reported. Nonetheless, many insurers still decide to use a broker tools as part of their flood risk analyses, since no better alternative is at hand. The next few paragraphs will explain how the broker tool can be used to derive a realistic expected flood claim, both in the current and future scenario.

A broker model often reports on a current damage factor, $Damage\ factor_{current,RP}$, associated with a specific return period (RP). This factor takes into account both the current probability of flooding (cfr. exposure: selecting the buildings at risk) and the damage when flooded (cfr. vulnerability). Therefore, we cannot apply this damage factor to the $VMM\ Exposure_{current,RP}$, as defined in section 3.1.2, since it would double count the selection of buildings at risk. We only want the vulnerability part of this factor. Unfortunately, the broker is not always able to decouple the vulnerability part from the exposure part.

Hence, we proceed as follows. Instead of selecting the at-risk properties and determining their exposure, we use the total fire insurance portfolio, containing N insured buildings such that:

$$Total\ exposure_{current} = \sum_{i=1}^{N} sum\ insured_i.$$

(Equation 4)

This formula looks very similar to Equation 3. However, the difference is that the index in Equation 4 runs over all buildings covered for flood, while Equation 3 considers only at-risk properties. We can then apply the $Damage\ factor_{current,RP}$ to this value without the risk of double counting the exposure part. We then find under the current scenario for a specific RP that the broker expects the total yearly claim size to be:

$$E\left(Total\ flood\ claim_{current,RP}\right) = Damage\ factor_{current,RP} \cdot Total\ exposure_{current}.$$

(Equation 5)

This is the total value of flood claims that we expect to receive in a year in the current scenario.

We cannot use the same method to calculate $E\left(Total\ flood\ claim_{future,RP}\right)$, i.e., the yearly total flood claim we expect by 2050, taking into account climate change, since broker tools often do not report on a future damage factor. Hence, to calculate future expected claim we propose to use the evolution between the current and future VMM flood exposure levels (see Equation 2) as proxy for the evolution in expected flood claims due to climate change. We call it the current-future factor. It can be calculated as

$$factor_{current-future,RP} = \frac{VMM\ exposure_{future,RP} - VMM\ exposure_{current,RP}}{VMM\ exposure_{current,RP}}.$$

Depending on the return period, this factor is between 110 % and 180% in Flanders. We can deduct from this that the VMM maps expects climate change to more than double the flood exposure by 2050. Consequently, we also assume that claims will more than double due to climate change. Hence, The total amount of future expected claims under the VMM map with specific RP is

$$E(Total\ flood\ claim_{future,RP}) =$$

$$E(Total\ flood\ claim_{current,RP}) * factor_{current-future,RP}.$$

3.1.4 Drawbacks of the black box broker model approach

The black box approach has some significant drawbacks. The next paragraph will discuss them and point out how the white box model will improve on them.

Firstly, the expected claim, $E(Total\ flood\ claim_{\ current,RP})$, is calculated applying some black box broker factor on the total Belgian exposure. Consequently, the expected claim does not take into account the vulnerability of the specific buildings at risk. The VMM maps are only used to get insight into the evolution of the exposure due to climate change, via the $Damage\ factor_{current,future}$. A more granular and accurate approach would be to quantify the vulnerability of those buildings affected by flood in the VMM maps. That is why this paper proposes to use depth-damage functions to model their vulnerability. This will be the topic of section 3.2.3. Secondly, the black box approach relies significantly on the availability of future flood hazard maps. This is no issue for Flanders since future flood maps are available. However, in many other regions and countries no maps are present. Some examples are Hungary, Wallonia and Czechia. Hence, the analysis is not generally applicable. For this reason, we propose to use the JRC maps instead and develop forward looking flood maps as set out in chapter 2. Finally, the VMM maps do not provide much insight into which climate change assumptions lead to the realization of its future maps. Since substantial uncertainty surrounds the evolution of climate change, and many pathways are still possible depending on future actions, more insights can be gained when using a climate framework. That is why this paper proposes to use the NGFS framework, as introduced in section 1.2. We will construct future maps based on the current policies, net zero 2050 and delayed transition climate pathway assumptions.

3.2 A white box model approach

3.2.1 Hazard: JRC maps and extension

The hazard is now modeled using the JRC flood hazard maps. Only current maps are available at the moment of writing. Therefore, we will use the future flood hazard maps as constructed in chapter 2 to represent future flood hazard. The flood maps are present for one in 10, 100, and 500 year return periods. The 10 year map can be consulted in Figure 37. It is colored light blue. This are the areas in Flanders the JRC believes are at risk for a 10 year flood. We also displayed one of the future maps, as build under chapter 2, namely the current policies 2050. The areas which become at risk in this scenario are dark blue.

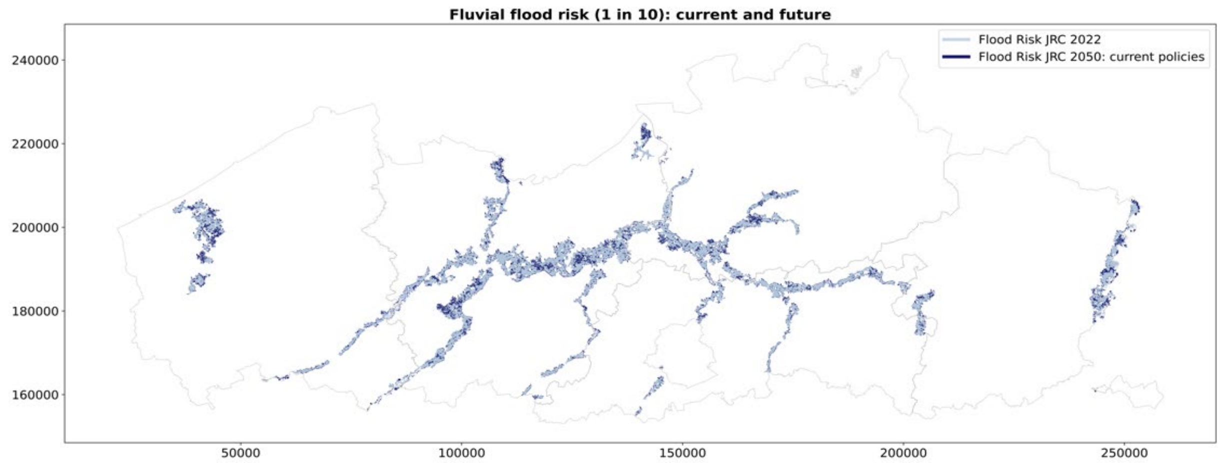

Figure 37: 10 year fluvial flood risk exposure in Flanders as provided by the JRC.

3.2.2 Exposure

As was the case in the previous methodology, the exposure is modeled using the insurer's fire insurance portfolio. Similar steps were also performed to select all buildings located in at-risk areas.

3.2.3 Vulnerability: depth - damage functions

Section 3.1.5 pointed out that the black box approach did not quantify the vulnerability of the specific buildings at risk. Instead, a black box factor was used. This paper proposes to use depth-damage functions instead. This more granular white box approach will allow to get more insight into the components of the vulnerability. Two significant insights can be, for example, the type of building (commercial, industrial, …) that is mainly affected or the cities where the buildings are most badly damaged.

As described in section 1.3.3, depth-damage functions are univariable loss models that relate the damage of a building and its household to the severity of the flood expressed in inundation depth. These functions can be empirically derived from loss datasets. However, insurers often do not have the necessary data to calibrate these curves. Hence, this paper proposes to work with the curves as provided by the JRC (Huizinga et al., 2017). These curves were developed because most regions or countries in Europe do not provide national ones. The depth-damage functions are available for a wide array of countries, but more general European curves are also present. Since JRC provides Belgian curves, we chose to work with these more granular country-specific curves. Huizinga et al. have also distinguished between industrial, commercial, and residential buildings. This distinction is very important as it allows insurers to more accurately differentiate between the buildings in their fire insurance portfolio. This, in turn, will lead to a more accurate damage assessment as well as allow to get more insight into which type of building accounts for most of the damages.

We will now detail how we calculate the $E(Total\ flood\ claim_{current,RP})$ by applying the depth-damage curves as introduced in section 1.3.3 on the buildings at risk. We proceed as follows. We first calculate the intensity of the flood at the location of the flooded property. This can be derived from the depth of the JRC flood polygon, $depth_{flood}$, the property is located in. Using the JRC curves, we can then transform this $depth_{flood}$ into a depth-damage factor, $Damage\ factor_{RP}$. Next, this factor is applied to the property's $sum\ insured$ to calculate the expected flood claim. We retake Equation 1 from section 1.3.3 to illustrate the method. Suppose that the depth-damage curve is characterized by the following equation:

$$Damage\ factor_{RP} = \begin{cases} x\ \% * SI\ \ if\ flood\ depth < a\ m \\ y\ \% * SI\ if\ \ a\ m \leq flood\ depth < a + 1\ m, \\ z\ \% * SI\ \ if\ flood\ depth \geq a + 1\ m \end{cases}$$

$$with\ 0 \leq x, y, z \leq 100\ \ and\ \ a \geq 0.$$

Suppose further that building i in the fire insurance portfolio is flooded by $a + 0.5\ m$ of water under the current 10 year JRC map. Its $Damage\ factor_{RP}$ is then equal to $y\%$, since the $\mathrm{flood\ depth}$ is in between $\mathrm{a\ m}$ and $\mathrm{a + 1\ m}$. Consequently, the expected damage to building i amounts to

$$E(flood\ claim_i) = Damagefactor_{RP,i} * \mathrm{sum\ insured_i}.$$

The total expected claim over all buildings can then be calculated as:

$$E(Total\ flood\ claim_{RP,current}) = \sum_{i=1}^{N} E(\ flood\ claim_i).$$

(Equation 6)

In this equation the index runs over all buildings located in JRC flooded areas having a return period of RP.

3.3 Comparison of both methodologies

Clearly, both approaches differ significantly. The next paragraphs will give some insight into the differences. We start by looking at the differences in flood maps used by the models. Next, we will investigate the difference in calculation of the vulnerability component.

3.3.1.1 Flood extent

The difference in extent between the flood maps is very significant. Figure 38 highlights this difference between the JRC current map (right most pane), used in the white box model and the VMM current map (left most pane), used in the black box model, on a smaller area. Both maps have a 10 year return period. The middle pane visualizes the overlap of both. Clearly, even the current maps, both input data, often do not predict the same areas to be flooded. Hence, it is not surprising that also the future maps, resulting from the current maps, will differ significantly. Unfortunately, this has considerable implications on the results as well, making it difficult to compare the two.

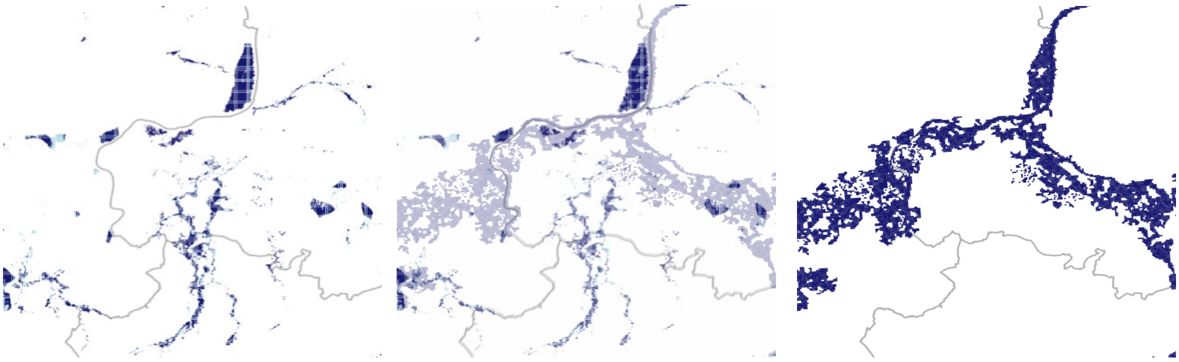

Figure 38: Illustration on a small area of the difference in flood extent between VMM (most left) and JRC (most right) maps. The illustration in the middle shows the overlap between the two.

The difference in these maps can be attributed to several facts. We will list the three most important ones in the following paragraphs.

Firstly, the JRC maps do not consider any flood protection or flood mitigation measures, like dikes or water levees (Alfieri et al., 2014). The maps start from the assumption that the flood is so severe that all flood protection fails. Thus, it really represents a worst-case scenario. The VMM maps, on the other hand, do take existing flood protection into account.

The second reason links to the granularity difference. The VMM maps can portray a more realistic view since they work on a more granular scale (2m vs. 100m). This allows them to more accurately describe flooded areas. A 100-meter granularity implies that the smallest flood in the JRC maps has a one 1 km^2 size, while the VMM can portray floods as small as 4 m^2. Consequently, even when only a smaller part is at risk, the JRC maps will catalog a much larger area as flooded. This lack of granularity is one of the downsides of working with cross-country flood maps.

Other flood maps try to alleviate some of these problems due to granularity by including a fraction variable (see e.g. ECB, 2021). This indicates how much of the area is in fact flooded. However, the JRC maps that are publicly available do not report on this value.

The last reason originates in one of the assumptions made by the creators of the JRC maps. They decided to only include the flood risk caused by those rivers having a large upstream area (Alfieri et al., 2014). Hence, all smaller streams or other water bodies are not displayed. The VMM, on the other hand, does not make this distinction. This is again linked to the granularity of the maps. The JRC maps would overestimate flood risk too much, representing flood risk in small streams by 1 km^2 flood polygons.

3.3.1.2 Vulnerability component

This paper proposed to replace the broker-damage factor with dept-damage functions to calculate the expected flood claims. This adaptation significantly increases the transparency of the results compared to the black box broker factor. We can now explore which building types are most at risk or contribute most to the total claim size. This approach allows for a more granular and exact view of the problem. However, this approach also tends to overestimate the actual damages. This has several reasons.

The first reason is directly linked to the granularity of the JRC maps. In these maps, each flood polygon has a uniform depth. On average, this amounts to 90 cm for the 1 in 10 year maps. Consequently, whenever the JRC maps predict a flood, an area of at least one km^2 is flooded with on average 90 cm of water. However, this would probably not mean that such a flood would be observed in real life. We would more likely observe a fraction of that area flooded with 90 cm in practice. Unfortunately, we are not able to make this distinction since no fraction variable is reported. Hence, buildings lying in areas that are less flooded than indicated by the JRC will contribute to overestimating the flood damages significantly.

A second reason is linked to the calibration of the functions. This paper has proposed to work with the functions as calibrated by the JRC since many insurers do not have enough data to calibrate it themselves. Consequently, it is challenging to verify whether those functions are close to an insurer's reality.

Due to these reasons, leading to a suspected overestimation of the risk, we propose to hold off using the depth-damage functions in official reporting to regulators until further research has been conducted.

4 Managing flood risk: the use of flood hazard maps in day-to-day business

Chapter 3 has provided ample evidence and arguments that flood risk is a significant climate risk that could negatively affect an insurers general performance if not properly managed. Hence, in this final chapter, we will discuss how an insurer can integrate fluvial flood maps, both current and future, in its daily processes and decisions, to manage the risk. The first part will look at underwriting, pricing, and acceptance processes. These are performed by the actuarial department. In the second part, we will shift our attention to the risk management side. We will investigate the four pillars that often make up its risk management: risk identification, -measurement, -appetite, and -reporting.

4.1 Acceptance, underwriting and pricing

The recent floods in Belgium clearly conveyed to insurers that large climate change induced flood events are more probable than initially perceived. Hence, offering clients a contract in line with their risk has become even more critical. To this extent, an insurer has multiple processes in place. We will give an example of how this could be implemented in practice by a Belgian insurer in the next paragraphs.

When a new client wants to take out fire insurance, his premium will be primarily based on the location and value of the property, and previous sustained flood damages.[8]

First, the insurer uses current flood hazard maps to assess whether the property is located in an at-risk zone. Based on this information, the property will then be assigned a risk zone number. The lowest risk zone means no flood risk and the area has never been flooded, while the highest indicates significant flood risk and actual flooding happened in the past. Secondly, based on some acceptance questions about the existence of past flood damages, a tariff class is assigned. Tariff one offers the best conditions, while the highest tariff class corresponds to risks the insurer deems too high to take on. These clients are referred to the 'Tariferingsbureau Natuurrampen'. This governmental organization offers coverage for flood at a reasonable premium fixed by law, and splits the risk amongst all Belgian insurer. Hence, it is based on a solidarity principle. Finally, the tariff, combined with the property's value, determines the premium.

[8] See, e.g., https://www.floodsmart.gov/what-impacts-my-premium-and-policy-costs

An existing client's premium can also be adapted. A higher tariff class can be assigned whenever a client changes risk zone due to an update of the current flood maps or when a flood event takes place.

Clearly, actuarial departments use current flood maps extensively to determine the risk of new and existing fire insurance policies. Namely, based on the location of the building, a risk zone is assigned. Hence, the quality and accuracy of these maps are paramount such that policies and tariffs reflect actual risk. Consequently, the JRC maps would not be a good fit for this application. The VMM maps, on the other hand, are much more appropriate. They could even be adapted to better fit historical observations. Areas that are low risk, according to the VMM, can then be assigned a more risky status if many past flood claims in that area are observed. This would, over time, create more realistic flood maps.

Future flood maps, as constructed in chapter 2, could also serve a purpose in underwriting and pricing. These maps could be used to evaluate trends in flood hazard areas. Based on these expected trends, premia could be adapted more smoothly. However, from a commercial point of view, we believe it will not be easy to introduce future maps in pricing since clients would not readily accept a higher premium for future risk. Especially since, in Belgium, fire insurance is a yearly renewable contract. Hence, updating premia at renewal on updated current maps would make more sense to clients. If multi-year contracts are introduced in the future, future flood maps could gain importance for the pricing of products.

4.2 Risk management

Risk management is an essential component of an insurer’s strategic management. It is often built around four pillars: risk identification, -measurement, -appetite, and -reporting. The goal is to adequately protect the company against volatile, adverse and unforeseen business environments. This safeguards the interests of all stakeholders involved, from employees and shareholders to the general economy.

Both prioritization by regulatory bodies and recent incidents like the exceptional rainfall resulting in disastrous floods in Western Europe during the summer of 2021 have made climate risk one of the top risks to manage. Especially flood risk is one of the natural catastrophe perils which is expected to be impacted significantly by climate change. Due to this risk's new nature, an increased effort has to be made to adapt existing processes and develop new climate tools that incorporate flood risk. In the following sections, we will elaborate on how flood maps can help in this respect. We will discuss its added value in each of the four pillars.

4.2.1 Pillar 1: risk identification

Risk identification is one of the cornerstones in risk management. It aims to identify possible risks at an early stage such that adequate mitigating actions can be taken. This allows an insurer to minimize or even avoid certain risks. Both new risks as well as shifts in existing risks are looked at. These risks can range from an evolution in flood risk to new upcoming legislation.

Both current and future flood maps can significantly add value in identifying (changes in) flood risk. Current maps can, for example, be used to assess how prone an insurer is in the short term to certain flood events. Even more important, changes in current maps, from year to year, can aid in understanding the present evolution of this risk. When current maps change significantly, this can be a clear risk signal to management that current pricing could no longer be adequate since it was based on maps that underestimated the current risk.

Future maps can also prove very valuable in identifying risks, especially when investigating a longer time horizon. Insurers often evaluate risks in 10 and 30 years' time. That is why this paper evaluated flood risk using 2032 and 2050 flood maps. The downside of these more extended time horizon maps is that many uncertainties surround them since they are based on expected future climate change. To cope with this difficulty, the maps were constructed for different NGFS climate scenarios. This allows management to get a broader view of the different identified risks.

Due to this uncertainty, the future maps will most likely not be used to base day-to-day management decisions on. However, they will prove valuable in identifying changes in flood risk to management.

4.2.2 Pillar 2: risk measurement

During risk measurement, an insurer aims to quantify the risks it is exposed to. Often risks identified during risk identification are selected to be examined. However, risk measurement can also serve as input for risk identification. If an analysis of a new kind of event, not yet identified as risky, points out the potential risk, it can be appropriately cataloged.

Multiple approaches exist to measure risks. The most straightforward approach is qualitative. Based on expert opinions and self-assessment, the potential impact is estimated. These opinions are underpinned using some qualitative methodology like literature reviews or interviews with experts. In the past, qualitative analyses were rarely used to measure risk. However, thanks to the initiation of climate exercises, this approach has seen an increase in interest. It is very well suited to capture a complex and uncertain topic like climate change.

A more challenging approach is to use mathematical models and algorithms to quantify the risks. These analyses often provide more actionable insights and are seen as more underpinned by regulators. However, model risk has to be considered when interpreting the results since no model can fully capture reality.

Based on the previous description of risk measurement, it is immediately apparent that flood maps can play a significant role in both the qualitative and quantitative measurement of flood risks. Qualitatively, the visual difference between current and future flood maps is valuable when underpinning the increased flood risk due to climate change. However, the real added value is that they provide the means to estimate flood risk quantitatively. Like in chapter 3, we can geo-map an insurer's flood exposure on the maps and calculate an expected future loss. This can give management insight into current and future proneness to flood risk.

We also believe insurers can create new climate metrics based on the future flood maps. An important candidate metric for this would be the combined ratio. A classic combined ratio relates the incurred claims and expenses over a year to the premiums earned as

$$Combined\ ratio_{current} = \frac{Claims_{incurred} + Expenses_{incurred}}{Premiums_{earned}}\ .$$

A ratio above one indicates that the insurer has made an underwriting loss. It is thus a measure of underwriting profitability.

We could transform this metric into a climate metric by replacing the flood $claims_{incurred}$ by the expected flood claims under the future flood maps and the premiums earned by the expected future premia. The formula would then become:

$$Combined\ ratio_{future} = \frac{Claims_{expected} + Expenses_{expected}}{Premiums_{expected}}.$$

This new metric could then be calculated for each different NGFS scenario and time horizon. This would allow an insurer to check which scenarios would lead to future unprofitable underwriting situations. This would make it easier for management to timely adapt pricing, underwriting and reinsurance policies when one of the scenarios unfolds.

4.2.3 Pillar 3: risk appetite

The risk appetite sets the boundaries of how much risk an insurer is willing to take. In practice, this often translates to setting limits for each group of risks the company is facing. Periodically, insurers then check whether all boundaries are still respected.

The risk appetite is still often set taking a short-term view into account. However, such a short time horizon can prove inadequate when evaluating climate risks due to the slow propagation of climate change effects. That is why it is important to also consider longer time horizons to fully capture these risks.

Clearly, the flood risk measurements and metrics mentioned in section 4.2.2 can serve as an input to set the risk appetite or detect breaches. Underwriting risk is an obvious candidate for which this is the case. As explained in the previous section, expected flood claims could help an insurer understand how their underwriting profitability could be impacted by climate change. Moreover, the flood maps themselves could also prove helpful in, for example, the calculation of credit risk profiles. Insurers could, for example, perform some analyses using flood maps to calculate a flood risk-adjusted Loan-to-Value (LTV). Based on this information they could argue that adaptation of underwriting policies or risk profiles are needed.

4.2.4 Pillar 4: risk reporting

The last pillar of the strategic risk management relates to reporting of risks. This reporting should be as transparent as possible and tailored to different stakeholders like shareholders, management, or regulators.

It is apparent that this last pillar can also benefit from the flood maps. These maps are very visually intuitive to interpret. Hence, they can be used in a wide array of reporting tools. Not only subject matter experts can understand and get valuable insights from them. Moreover, since the flood maps proved to have significant added value in the risk identification, measurement, and appetite pillars, a more accurate view of the risks can be reported.

Conclusion and further research

In recent years, flood risk has become top of mind at insurance companies. A prioritization by regulatory bodies as well as recent flood events, showing insurers proneness to flood, have made it one of the top risks to manage. Moreover, flood risk assessments, like the one performed in chapter 3, have indicated that flood events could have a significant impact on insurers' underwriting profitability.

Flood maps are an essential tool in managing this risk. They are used when performing flood analyses. Flood maps provide insight in the probability and severity of flood events. Both current and future maps exist. Future flood maps differ from current ones, since they take into account a best estimate of the future climatological situation. Hence, they provide a forward looking view. They are essential in determining future flood risk.

However, these future maps are often not publicly available. For this reason, this paper has developed an algorithm to construct forward looking flood maps from the JRC current flood hazard maps since these are publicly available and endorsed by regulators. We relied on an interpolation technique to make the current maps forward looking.

The algorithm has a lot of strengths. It is able to create cross-border future maps using a limited amount of time and computing power. All data used is also publicly available. This ensures that insurers are not dependent on the goodwill of local governments. It is also a white box method. It is easy to understand, interpret and visualize the results.

Unfortunately, the resulting flood maps also display significant weaknesses. The most important one is its granularity. The JRC maps can only display floods up to $100m$ granularity. In comparison, official flood hazard maps often achieve a granularity of $2m$. This limited granularity can lead to a reduced accuracy in flat lowland or mountainous areas. This specific geography can lead to, for example, floods extending for many kilometers after only a small increase of the flood depth. It can also prohibit the algorithm to capture all relevant flooded areas.

The algorithm is also very sensitive to how the modeler thinks the flood intensity will evolve due to climate change. This is captured by the model in an 'increase in flood depth' variable. This paper has proposed to use data provided by the NGO climate analytics as a proxy. They are a well-regarded institution supported by a wide variety of universities and institutions like the JRC and EIOPA. However, climate analytics does not provide insight into their assumptions and methods of calculating this evolution in flood depth. They also do not provide data on some Central-European countries like Slovakia. Since the results are highly dependent on this variable, some more research should be done in defining a realistic value.

Much uncertainty surrounds climate change and, more specifically, flood events. Hence, it is challenging for practitioners to evaluate the accuracy of flood maps. So, caution should be taken when choosing one of the flood maps over the other.

To cope with this uncertainty, this paper proposes to continue working with both the JRC maps and the VMM maps. Being aware of their shortcomings and strengths, we believe they both can add value to an insurer's daily processes and strategic management. Thanks to the high granularity, the VMM maps, for example, can serve a purpose in pricing and underwriting exercises. In these, accuracy is paramount. Moreover, the JRC maps can add value in stress testing since they depict a worst-case scenario where all flood defenses fail. This can also lead to interesting insights.

This paper also proposes to keep challenging the maps and results using historical data. No map displays reality best. It is important to know which map displays which situation best. This can only be achieved when more high-quality historical data is available.

Future work could build on this study by adapting the flood maps to better fit historical claims. This would allow for a more realist view on an insurer's exposure. One could also investigate whether the JRC and VMM maps could be combined. This could lead to maps having both a nice granularity and a large geographical use.

List of figures

List of tables

Sources

Articles

Abrams, M. (2000). *The Advanced Spaceborne Thermal Emission and Reflection Radiometer (ASTER): Data products for the high spatial resolution imager on NASA's Terra platform. International Journal of Remote Sensing*, 21(5), 847–859. https://doi.org/10.1080/014311600210326

Alfieri, L., Salamon, P., Bianchi, A., Neal, J., Bates, P., & Feyen, L. (2014). Advances in pan-European flood hazard mapping: *ADVANCES IN PAN-EUROPEAN FLOOD HAZARD MAPPING*. *Hydrological Processes*, *28*(13), 4067–4077. https://doi.org/10.1002/hyp.9947

Apel, H., Aronica, G. T., Kreibich, H., & Thieken, A. H. (2009). *Flood risk analyses—how detailed do we need to be?* Natural Hazards, 49(1), 79–98. https://doi.org/10.1007/s11069-008-9277-8

Balica, S. F., Popescu, I., Beevers, L., & Wright, N. G. (2013). *Parametric and physically based modelling techniques for flood risk and vulnerability assessment: A comparison. Environmental Modelling & Software*, *41*, 84–92. https://doi.org/10.1016/j.envsoft.2012.11.002

Bongiorno, L., Claringbold, A., Eichler, L., Jones, C., Kramer, B., Pryor, L., & Spencer, N. (2022). *Climate scenario analysis for pension schemes: A UK case study*. British Actuarial Journal, 27, E6. https://doi.org/10.1017/S1357321721000106

Brown, O. L. I. (1951). *The Clausius-Clapeyron equation*. Journal of Chemical Education, 28(8), 428. https://doi.org/10.1021/ed028p428

Delcea, R. (2020, December 2). *Discussion Paper: Methodology on potential inclusion of climate change in the nat cat standard formula* [Text]. Eiopa - European Commission. https://www.eiopa.europa.eu/document-library/consultation/discussion-paper-methodology-potential-inclusion-of-climate-change-nat_en

Delcea, R. (2021, April 19). *Opinion on the supervision of use climate change risk scenarios in ORSA* [Text]. Eiopa - European Commission. https://www.eiopa.europa.eu/document-library/opinion/opinion-supervision-of-use-of-climate-change-risk-scenarios-orsa_en

Dottori, F., Mentaschi, L., Bianchi, A. (2020). *Adapting to rising river flood risk in the EU under climate change : JRC PESETA IV project : Task 5*. European Commission. Joint Research Centre. https://data.europa.eu/doi/10.2760/14505

Dufourmont, H., Gallego, J., Reuter, H., & Strobl, P. (2014*). EU-DEM Statistical Validation*. https://ec.europa.eu/eurostat/documents/7116161/7172326/Report-EU-DEM-statistical-validation-August2014.pdf

ECB. (2021). *Climate-related risk and financial stability.* https://www.ecb.europa.eu/pub/pdf/other/ecb.climateriskfinancialstability202107~87822fae81.en.pdf

Eiopa. (2021). Consultation on Application guidance running climate change materiality assessment and using scenarios in the ORSA Cons. https://www.eiopa.europa.eu/document-library/consultation/consultation-application-guidance-running-climate-change-materiality-0_en

Ford, D., Ashton, B., Audley, K., Qazvini, M., Yuan, Y., McLintock, Y. (2019). Practical guide to climate change for life Actuaries., https://www.actuaries.org.uk/system/files/field/document/A%20Practical%20Guide%20to%20Climate%20Change%20%20for%20Life%20actuaries%20-%20Oct%20v7a.pdf

Gerl, T., Kreibich, H., Franco, G., Marechal, D., & Schröter, K. (2016). *A Review of Flood Loss Models as Basis for Harmonization and Benchmarking*. *PLOS ONE*, *11*(7), e0159791. https://doi.org/10.1371/journal.pone.0159791

Homer, D., Li, M. (2017). *Notes on Using Property Catastrophe Model Results*. Society of Actuaries in Ireland. https://web.actuaries.ie/node/178516

Humphreys, N. (2020). *Exceedance Probability in Catastrophe Modeling*. Casualty Actuarial Society E-Forum, Winter 2021. https://www.casact.org/sites/default/files/2021-03/02_humphreys.pdf

Huizinga, J., de Moel, H. , Szewczyk, W. (2017). *Global flood depth-damage functions. Methodology and the database with guidelines*. EUR 28552 EN. https://op.europa.eu/s/v6Kx

International Actuarial Association (2017). *Climate Change and Mortality,* https://www.actuaries.org/CTTEES_ENVIRO/Papers/REWG_CCandMortality_final_Nov2017.pdf

IFoA (2017). *Climate Risk Alert*, https://www.actuaries.org.uk/news-and-insights/media-centre/media-releases-and-statements/ifoa-warns-climate-change-financial-risks

IPCC (2022). *Climate Change 2022: Impacts, Adaptation, and Vulnerability. Contribution of Working Group II to the Sixth Assessment Report of the Intergovernmental Panel on Climate Change* [H.-O. Pörtner, D.C. Roberts, M. Tignor, E.S. Poloczanska, K. Mintenbeck, A. Alegría, M. Craig, S. Langsdorf, S. Löschke, V. Möller, A. Okem, B. Rama (eds.)]. Cambridge University Press. In Press.

https://www.ipcc.ch/report/ar6/wg2/downloads/report/IPCC_AR6_WGII_FinalDraft_FullReport.pdf

Kron, W. (2005). *Flood Risk = Hazard • Values • Vulnerability*. *Water International*, *30*(1), 58–68. https://doi.org/10.1080/02508060508691837

Mason, D., Garcia-Pintado, J., Cloke, H., & Dance, S. (2015). *The potential of flood forecasting using a variable-resolution global Digital Terrain Model and flood extents from Synthetic Aperture Radar images.* Frontiers in Earth Science, 3, 43. https://doi.org/10.3389/feart.2015.00043

Mediero, L., Garrote, L., Santillán, D., Cueto-Felgueroso, L., & Soriano, E. (2021). *Discharge-damage curve and EAD estimates in the Pamplona metropolitan area (Spain) by using insurance data*. *Science and Practice for an Uncertain Future*, null-null. https://doi.org/10.3311/FloodRisk2020.7.3

de Moel, H., van Alphen, J., & Aerts, J. C. J. H. (2009). *Flood maps in Europe – methods, availability and use.* Natural Hazards and Earth System Sciences, *9*(2), 289–301. https://doi.org/10.5194/nhess-9-289-2009

Molinari, D., Scorzini, A. R., Arrighi, C., Carisi, F., Castelli, F., Domeneghetti, A., Gallazzi, A., Galliani, M., Grelot, F., Kellermann, P., Kreibich, H., Mohor, G. S., Mosimann, M., Natho, S., Richert, C., Schroeter, K., Thieken, A. H., Zischg, A. P., & Ballio, F. (2020). *Are flood damage models converging to "reality"? Lessons learnt from a blind test*. *Natural Hazards and Earth System Sciences*, *20*(11), 2997–3017. https://doi.org/10.5194/nhess-20-2997-2020

Papathoma-Köhle, M., Zischg, A., Fuchs, S., Glade, T., & Keiler, M. (2015). *Loss estimation for landslides in mountain areas – An integrated toolbox for vulnerability assessment and damage documentation*. *Environmental Modelling & Software*, *63*, 156–169. https://doi.org/10.1016/j.envsoft.2014.10.003

Rabus, B., Eineder, M., Roth, A., & Bamler, R. (2003). *The shuttle radar topography mission—a new class of digital elevation models acquired by spaceborne radar*. ISPRS Journal of Photogrammetry and Remote Sensing, 57(4), 241–262. https://doi.org/10.1016/S0924-2716(02)00124-7

Risser, M. D., & Wehner, M. F. (2017). *Attributable Human-Induced Changes in the Likelihood and Magnitude of the Observed Extreme Precipitation during Hurricane Harvey. Geophysical Research Letters*, *44*(24), 12,457-12,464. https://doi.org/10.1002/2017GL075888

Rothwell, M., Earle, M., Ooi, C. H., Orr, J., Shroff, S., & Siew, J. (2020). Practical guide to climate change for general insurance practitioners. British Actuarial journal, 25. https://doi.org/10.1017/S1357321720000136

Sampson, C. C., Smith, A. M., Bates, P. D., Neal, J. C., & Trigg, M. A. (2016). *Perspectives on Open Access High Resolution Digital Elevation Models to Produce*

Global Flood Hazard Layers. Frontiers in Earth Science, 3, 85. https://doi.org/10.3389/feart.2015.00085

Tesselaar, M., Botzen, W. J. W., & Aerts, J. C. J. H. (2020). *Impacts of Climate Change and Remote Natural Catastrophes on EU Flood Insurance Markets: An Analysis of Soft and Hard Reinsurance Markets for Flood Coverage*. Atmosphere, 11(2), 146. https://doi.org/10.3390/atmos11020146

Wright, D. B. (2015). *Methods in Flood Hazard and Risk Assessment*. World Bank. https://openknowledge.worldbank.org/handle/10986/22982

Yamazaki, D., Ikeshima, D., Tawatari, R., Yamaguchi, T., O'Loughlin, F., Neal, J. C., Sampson, C. C., Kanae, S., & Bates, P. D. (2017). *A high-accuracy map of global terrain elevations: Accurate Global Terrain Elevation map*. Geophysical Research Letters, 44(11), 5844–5853. https://doi.org/10.1002/2017GL072874

Internet

Federal Emergency Management Agency. (n.d.). *What impacts flood insurance policy costs?*. Floodsmart. Retrieved 20 April, 2022 fromhttps://www.floodsmart.gov/what-impacts-my-premium-and-policy-costs

Massam, A. (2020, April 15). *The physics of Precipitation in a Warming Climate. JBA risk management*. Retrieved March 18, 2022 from https://www.jbarisk.com/news-blogs/the-physics-of-precipitation-in-a-warming-climate/

Vlaamse Milieu Maatschappij. (n.d.). *Overstromingen*. Retrieved April 11, 2022, from https://klimaat.vmm.be/themas/overstromingen

Coördinatiecommissie Integraal Waterbeleid (CIW). (n.d). *De overstromingskaarten uitgelegd*. Retrieved April 26, 2022, from https://www.integraalwaterbeleid.be/nl/beleidsinstrumenten/watertoets/overstromingskaarten

Coördinatiecommissie Integraal Waterbeleid (CIW). (2011, November 3). *Overstromingsveilig bouwen en wonen.* Retrieved April 20, 2022, from https://www.integraalwaterbeleid.be/nl/publicaties/afbeeldingen/Overstromingsveilig%20bouwen%20en%20wonen%20-%20CIW.pdf

Data Set

Copernicus Program. (2016). *EU-DEM (LAEA) (Version 1.1)* [Data set]. Retrieved October 12, 2021, from https://land.copernicus.eu/imagery-in-situ/eu-dem

Dottori, F., Alfieri, L., Bianchi, A., Skoien, J., Salamon, P., (2021). *River flood hazard maps for Europe and the Mediterranean Basin region. European Commission, Joint Research Centre (JRC)* [Data set]. Retrieved October 12, 2021, from http://data.europa.eu/89h/1d128b6c-a4ee-4858-9e34-6210707f3c81

Vlaamse Milieu Maatschappij. (2021). Overstromingsrisicokaarten - Fluviaal: globale_risicokaart [Data set]. Retrieved October 14, 2021, from https://geoservice.waterinfo.be/web/

FACULTY OF BUSINESS AND ECONOMICS
Naamsestraat 69 bus 3500
3000 LEUVEN, België
tel. + 32 16 32 66 12
fax + 32 16 32 67 91
feb.leuven@kuleuven.be
www.feb.kuleuven.be